UNIVERSITA' DEGLI STUDI DI TORINO

Scardia et al. (2014) -Geological Society of America Bulletin, v.127 (1/2), 113-130

doi: 10.1130/B30990.1

Scardia et al., 2014, Geological Society of America Bulletin, Doi: 10.1130/B30990.1

Evidence for late Alpine tectonics in the Lake Garda area (northern Italy) and seismogenic implications

Giancarlo Scardia*
Istituto di Geologia Ambientale e Geoingegneria – CNR, via Salaria km 29.300, I-00016 Monterotondo Scalo (Roma), Italy.

Andrea Festa
Dipartimento di Scienze della Terra, Università di Torino, Via Valperga Caluso 35, I-10125 Torino, Italy.

Giovanni Monegato
Istituto di Geoscienze e Georisorse – CNR, via Valperga Caluso 35, I-10123 Torino, Italy.

Roberta Pini
Istituto per la Dinamica dei Processi Ambientali – CNR, Piazza della Scienza 1, I-20126 Milano, Italy.

Sergio Rogledi
ENI E&P, via Emilia 1, I-20097 San Donato Milanese, Italy.

Fabrizio Tremolada
RPS Energy, Goldsworth House, Denton Way, Goldsworth Park, GU213LG Woking, UK.

Fabrizio Galadini
Istituto Nazionale di Geofisica e Vulcanologia, via di Vigna Murata 605, I-00143 Roma, Italy.

* corresponding author: scardia@usp.br
Present affiliation: Instituto Oceanográfico, Universidade de São Paulo, Praça do Oceanográfico 191, São Paulo, SP 05508-120, Brazil

Abstract

We investigated the recent evolution of the Po Plain-Alps system by integrating subsurface geophysical data from the Po Plain with new stratigraphic and structural observations from the Southern Alps margin. Inversion of structural data and chronology provided by stratigraphic constraints led to the definition of three tectonic events since the Pliocene – namely the intra-Zanclean, the Gelasian, and the Middle Pleistocene –, driven by an axis of maximum compression formerly oriented at NE (intra-Zanclean) and then to NNW (Gelasian and Middle Pleistocene). The associated deformation has been accommodated by two sets of faults consisting of NNE-trending thrust faults, mostly represented in the western sector of the Lake Garda, and NW-trending strike-slip faults, observed in the southern and eastern sector. The interplay between these two sets of faults is interpreted to produce relatively short (< 10 km length) thrust ramps activated in left transpression, bounded by relatively longer (30-60 km) transfer faults activated in a right lateral strike-slip motion. Basing on this structural model, we infer moderate seismicity (M_w < 6) associated to the NNE-directed thrusts and stronger earthquakes (also M_w > 6.5) along the NW-trending strike-slip faults. In this framework, the newly defined Nogara Fault or the Sant'Ambrogio Fault, all pertaining to the NW-trending system, are regarded as a potential candidate for the seismogenic source of the January 1117 event, the most destructive earthquake in the Po Plain.

Keywords: Pleistocene, stratigraphy, active tectonics, Po Plain, Alps, Italy.

1. Introduction

After a complex succession of deformation phases, traditional geologic view constrains the end of the Alpine tectonics in the Po Plain to the late Messinian (Pieri and Groppi, 1981; Castellarin et al., 1992; Fantoni et al., 2004), with residual activity confined in the eastern Southern Alps (e.g., Castellarin and Cantelli, 2000; Galadini et al., 2005). This view mainly relies on the occurrence of post-orogenic Pliocene marine deposits sealing the folded and eroded Meso-Cenozoic Alpine bedrock (Castellarin et al., 1992). However geomorphologic, seismological, and geodetic evidence (e.g., Desio, 1965; Anderson and Jackson, 1987; D'Agostino et al., 2008; Livio et al., 2009) clearly points to a still on-going deformation in Southern Alps and Po Plain, the study of which is the aim of the present work.

Increasing scientific sensibility on the seismic hazard of the Po Plain led to modern studies based on punctual paleoseismological investigations (Galadini and Galli, 1999; Galadini et al., 2001; Livio et al., 2009). Moving from these studies, our present work aims to depict a new structural model for the Po Plain that accounts for the largely ignored Plio-Pleistocene tectonics of the Southern Alps and its seismogenic implications at regional scale. A special emphasis is given to the Lake Garda area because of i) its structural complexity as interference area between two different structural styles, ii) the occurrence of deformed Pliocene–Pleistocene deposits, and iii) the occurrence of damaging historical earthquakes (e.g., 1117, M_w 6.7; 1222, M_w 5.8; 1891, M_w 5.9; 1901, M_w 5.5; Guidoboni et al., 2007; Pessina et al., 2013). We base our study on the integration of subsurface geophysical data with new direct stratigraphic and structural observations, gathered by means of detailed geological survey along the Southern Alps margin. Taking into account that sedimentation (in the Po Plain) or erosion (in the Alps) rates are much higher than the tectonic strain rate (e.g., Livio et al., 2009; Burrato et al., 2012), we focused on the Pliocene and early Pleistocene deposits, where cumulative deformation is expected to be maximum.

2. Regional background

The tectonic setting of the Southern Alps was determined by a complex history including Mesozoic rifting and convergence between the European and Adriatic plates since Late Cretaceous. Thrusting of the Paleozoic basement and its sedimentary cover during the Miocene represented the final, post-collisional phase of the Alpine orogeny and resulted in the formation of a fold-and-thrust belt composed of south-verging thrust sheets (e.g., Laubscher, 1985; Picotti et al., 1995).

The Lake Garda area lies between two sectors characterized by different structural styles. To the west, the "Giudicarie belt" consists of NNE-trending transpressive thrusts and folds (Fig. 1). The eastern sector is characterized by the rigid block of the Lessini Mts., mainly deformed by the NW-trending, strike-slip "Schio-Vicenza" fault system. Since the late Messinian Apennines-related flexural subsidence involved the southern sector of the Alps, resulting in the southward tilting and burial of the outermost Alpine thrusts (e.g., Fantoni et al., 2004). Southward tilting also involved the former Alpine foreland producing a regional monocline dipping ~5° toward the Apennines (Mantova Monocline; Fig. 1). During the Pliocene and the early Pleistocene – now including the Gelasian stage (Gibbard et al., 2010) – the step-wise northward migration of the Apennines produced basin-wide structural modifications and the deposition of two tectono-stratigraphic groups – namely EP (Pliocene) and LP (Pleistocene) – produced by the intra-Zanclean and Gelasian tectonic phases, respectively (Ghielmi et al., 2010). After the severe Pliocene tectonics, a gradual decrease of the Apennines compressional deformation occurred during the early Pleistocene as indicated by the reduced growth of the existing structures (Ghielmi et al., 2010). A probably associated decrease in subsidence led the Po basin to the complete infilling (sequences PS1–PS3 within LP group; Scardia et al., 2012).

In a context of low deformation rates, the climatic signal becomes evident in the stratigraphic record of the Po Plain with the formation of the R surface (base of sequence PS2), a regional seismic horizon which marks the onset of the major Pleistocene glaciations at ~0.9 Ma (Muttoni et al., 2003). Since the Middle Pleistocene, the outward migration of the Apennines seems to stall and no formation of new thrusts is documented (Picotti and Pazzaglia, 2008). Broadly at the same time, erosion-driven isostatic rebound is inferred to be the dominant process in the western Southern Alps (Scardia et al., 2006; 2012). Associated decreasing in accommodation space forced fluvial systems to prograde basinward triggering the formation of the Y surface (base of PS3 sequence) at ~0.45 Ma (Scardia et al., 2012).

Land exposures preserve a fragmentary and marginal record of the Plio-Pleistocene events, making their remarkable and direct information very scattered. Sparse Pliocene deposits and late Cenozoic conglomerates are known along the Alpine margin since early studies (see section 3) and their revision by the present study is aimed to frame them in the above-mentioned regional stratigraphic layout, with the mutual advantage provided by the better chronological constraints of the outcrops and the stratigraphic continuity of the subsurface stratigraphy.

3. Subsurface geology

The subsurface geologic structure of the Po Plain has been depicted in the early 80s by Pieri and Groppi (1981). A recent reappraisal summarized in Fantoni et al. (2004) mainly dealt with the western and central sectors of the buried Southern Alps front. Moving from these studies we re-interpreted the whole ENI seismic dataset of the central and eastern Po Plain, focusing on the largely ignored Mantova Monocline (Fig. 1). Following the approach of Fantoni et al. (2004), we mapped the main buried structural features at different stratigraphic levels, projecting onto the horizontal plane the hanging-wall cutoffs at the Aptian-Albian unconformity (top of the Mesozoic

calcareous rocks) and at the youngest horizon (Messinian to early Pliocene) of the Cenozoic terrigenous units (Fig. 1). Differences in some details between the structures mapped in Figure 1 and those from previous studies are ascribable to a different interpretation of seismic data and to the application of slightly different models of structural style.

3.1 Southern Alps structures

The northern sector of the Po Plain is characterized by the occurrence of the Southern Alps buried fronts, which interact in their outermost portion with the Apennines fronts. The interaction takes place along a deeper, E-W oriented paleo-structure (the Corneliano-Bordolano axis; Fig. 1), representing a residual foreland comprised between the Southern Alps and the Apennines thrusts. The Southern Alps are characterized by two different structural styles. Between Lake Como and Lake Iseo deformation consists of imbricate south-verging thrusts, involving both the Mesozoic calcareous succession and the overlying Cenozoic terrigenous deposits. The metamorphic basement seems to be clearly involved only northwards of the Franciacorta and Brescia faults (Fantoni et al., 2004; Fig. 1), where low-angle detachment planes can be observed at relatively shallow depth.

South of Lake Iseo, the Southern Alps structures experience abrupt rotations or interruptions (Fig. 1). This behavior is attributed to an inherited, deeper, NNE-trending fault rooted in the basement (Iseo Fault, Fig. 1; see also section 12 of Pieri and Groppi [1981] and Fig. 7a of Fantoni and Franciosi [2010]). The Iseo Fault corresponds to a major extensional fault of Mesozoic or Permian age, already inferred in literature from land exposures (i.e., Lake Iseo-Oglio River line [Castellarin et al., 1992], Sebino Faults [Bertotti et al., 1993], Val Camonica line [Cassinis and Perotti, 1996]). East of this fault, the Southern Alps south-verging thrusts in Cenozoic terrigenous units shift to one (Fantoni et al., 2004) or two major, north-verging back-thrusts (Livio et al., 2009), reflecting a different arrangement of the deeper structures and, ultimately, a paleogeographic conditioning (see also Ravaglia et al., 2006).

More eastward, in the Lake Garda area, the Alpine thrusts evolve in lateral ramps according to a NNE-trend (Fig. 1). Here, the decreasing offset in the outermost structures records the transition to the foreland, where incipient, high-angle faults show a slight inversion of the movement with respect to their former Mesozoic extensional behavior (Solferino Fault; Figs. 1, 2A). Interpretation of the available seismic lines shows for the NE-trending Sirmione Fault a vertical offset of ~2 km (~1 two-way time seconds at ~4 km/s; Fig. 2A). This fault is correlative of the inferred structure known in literature as Sirmione-Garda fault (Carton and Castaldini, 1985, and reference therein). Plio-Pleistocene seismic reflectors in the Lake Garda area are poorly imaged in the available seismic profiles, but some disturbance along the Sirmione Fault seems to occur up to the level of the R surface (base of the PS2, ~0.9 Ma; Fig. 2A), with the western sector uplifted with regards to the eastern sector.

On the whole, abrupt changes in striking and dipping of faults at shallow depths suggest a control exerted by lineaments pre-dating the Alpine compressional phases. These older faults may be reactivated or control the trajectory of newly formed faults. The structural elements controlling this behavior are Mesozoic extensional and transfer faults, often reactivated as lateral ramps of the new Alpine thrusts or accommodating the flexural tilting in the foreland sector. We also observe that thrusts in Cenozoic terrigenous units often develop frontal ramps in correspondence of the structural steps provided by the underlying Mesozoic normal faults (e.g., Piadena Fault; Fig. 1; see also Picotti et al., 2007).

2.2 Foreland structures

The present-day foreland is represented by the Mantova Monocline, a regional, south-dipping structure, which lies between the Alpine and Apennines fronts (Figs. 1, 2B). Interruptions and offsets in the Mesozoic reflectors point to the occurrence of blocks bounded by sub-vertical faults, as observed in the exposed area of Lessini Mts. The main structural setting consists of NW-oriented extensional faults, bounding tilted blocks of variable size and sometimes interrupted by

transfer faults (Figs. 1, 2B). All over the Mantova Monocline, relative highered and lowered blocks can be recognized in the Mesozoic succession. The lowered blocks identify more subsiding troughs like the Suzzara Basin, bounded eastward by the NW-trending Viadana Fault and interrupted northward by the NE-trending Mantova Fault (Fig. 1).

Among the NW-trending faults, the Nogara Fault (Figs. 1, 2B) appears to be the most notable. It consists of a sub-vertical plane that bears variable displacements often showing reversal of the downthrown and upthrown sides. This feature suggests a scissor fault behavior, characterized by a strike-slip deformation mechanism. The evidence of this fault is not always well traceable in the ENI seismic dataset, probably because the seismic resolution is about 20-30 m and it doesn't allow to detect relatively smaller offsets. The estimate length of this fault is ~60 km and in the best 2D seismic profile deformation or interruption of seismic reflectors seem to occur at least up to the Y surface (Fig. 2B).

3. Geology of land exposures

Geological survey was carried out on Pliocene and Early Pleistocene deposits of the Lake Garda area, with the aim of detecting evidence of faulting and constraining the age of deformation. We chose relatively older deposits with respect to the common practice in active tectonics studies (e.g., Galadini et al., 2012), because in an area where glacial erosion has been the main shaping process (with rates much higher than those related to the tectonic activity) only the few sparse remains of Plio-Pleistocene deposits may provide evidence of strain by cumulated deformation.

We present data from three sites distributed in the western side, eastern side, and the middle of the Lake Garda area, respectively (Fig. 1). These sites bear evidence of the different structural styles, i.e.:

- The western sector is mainly characterized by NNE-directed, SE-verging thrust faults belonging to the Giudicarie belt;
- The eastern sector, corresponding to Lessini Mts., consists of rigid blocks bounded by sub-vertical, NW/NNW strike-slip faults (Schio-Vicenza fault system);
- The central sector records the complex structural interference between the differently oriented fault systems above described, as observed northward in the Trento area.

These structural styles are also reflected in the seismotectonic settings of the Lake Garda area, where focal plane solutions document dominant contractional and strike-slip components in the Giudicarie belt and in the Lessini Mts. area, respectively (Viganò et al., 2008).

For chronostratigraphic considerations we refer to the Lourens et al. (2005) time scale, modified after Gibbard et al. (2010) and Backman et al. (2012).

3.1 Western sector

3.1.1 Stratigraphy

The area between Brescia and Lake Garda (Fig. 1) is characterized by the occurrence of isolated reliefs located south of Brescia and related to the growth of buried thrusts since at least the Middle Pleistocene (Desio, 1965). Moving along the western Lake Garda bank, Pliocene and Early Pleistocene deposits are exposed in few and sparse outcrops along eastern bank of Chiese River, where no significant deformation has been observed. The most striking evidence of late Alpine

tectonics in the western bank of Lake Garda is found at the San Bartolomeo Hill, where Pliocene marine deposits have been uplifted to an elevation of ~500 m above the sea level.

The San Bartolomeo Hill Formation (Baroni et al., 1995) consists of a transgressive-regressive cycle subdivided in three members, named SB1, SB2, and SB3 from bottom to top, respectively (Fig. 3). SB1 and SB3 display very similar lithology and petrography, and they can be separated with confidence only when the intermediate SB2 member occurs. The SB1 member may reach a maximum thickness of ~170-m-thick and consists of coarse-grained, massive to crudely bedded conglomerate, unconformably lying on the bedrock (Fig. 3). The conglomerate passes upward to 50-m thick, massive to laminated, fossiliferous silty clays (SB2). Toward the top, sand and gravel lenses are common, as well as intervals with a very thin lamination and organic-rich layers. The succession is sealed by a ~25-m-thick conglomerate (SB3), with roughly the same petrography composition of the underlying gravels. The boundary between the fine-grained deposits and the upper conglomerates is erosional. The latter sediments show an increasing organization toward the top, from crudely bedded and coarse-grained to horizontal or planar cross-bedded and medium- to fine-grained.

Clast petrography of the SB1 is dominated by dolostone fragments (57%) with the overall carbonates exceeding 80%; this composition points to a local drainage from the Southern Alps sedimentary cover (Fig. 4), also suggested by the ~50-cm-sized blocks of marly limestone ("scaglia" facies) observed at the base. The SB2 and SB3 members show a progressive enrichment in volcanic (> 10%) and metamorphic clasts (~5%), interpreted as a mixing of the local drainage with the wider Adige catchment (Tab. 1; Fig. 4).

Basing on facies analysis, the lower conglomerate SB1 is interpreted as an alluvial fan. Even if the boundary between this latter and the upper SB2 member is not observed, we interpret the fining upward trend of SB1 coupled with the occurrence of marine clays at the top (SB2) as a unique transgressive event. The coarsening upward at the top of SB2 and the very thin laminated organic-rich layers point to a gradual shallowing of the environment, from shelf to lagoon settings. Braidplain deposits of SB3 close the regressive sequence.

Calcareous nannofossil investigations have been performed on 12 samples collected in the SB2 marine deposits (Tab. 2). The analyzed samples show a scarce content in nannofossils, characterized by a moderate conservation and abundant reworked taxa from Mesozoic and Paleogene. All 4 samples collected in the northeastern sector of the San Bartolomeo Hill turned out to be barren and are not reported in Tab. 2. The presence of *Pseudoemiliania ovata*, *Sphenolithus abies*, and *P. lacunosa* allows assigning the SB2 member to the NN14–NN15 zone (Martini, 1971; 4.04–3.81 Ma, late Zanclean). In addition, the first occurrence of *P. lacunosa* at the top of the succession provides an age of 3.82 Ma (Backman et al., 2012).

Samples collected for pollen analysis in fine-grained levels of the lower SB1 conglomerate turned out to be devoid of pollen. One sample collected in the SB2 marine clays (Fig. 3, sample SB22) yielded limited pollen concentration (<1800 grains/cm^3 of sediment), but sufficient to provide basic paleoenvironmental and biostratigraphic information (Tab. 3). The pollen spectrum originates from conifer forests of cool climate, dominated by *Cathaya* (37% of the identified grains) accompanied by pines, spruce, and hemlock. Pollen of woody Angiosperms occurs as sporadic items. Precise biochronologic attribution is not possible with a single pollen spectrum, but some simple considerations can be derived: i) the abundance of *Cathaya* rules out any attribution to the early Pleistocene, ii) comparison with the available data from the Pliocene of northern Italy (Bertini, 2001) may suggest that sample SB22 deposited sometimes after 4 Ma and before 2.6 Ma, in good agreement with the nannofossil biostratigraphic data.

Basing on the latest Zanclean age of the whole SB2 member and its supposed continuity with the underlying SB1 in a unique transgressive event, we suggest an early Pliocene age for the lower conglomerate, in agreement with Cita (1955). Our interpretation differs from the latest Messinian age of Picotti et al. (1997), relying on the finding of *Melanopsis* sp. at the base of SB2. A generic *Melanopsis* has poor biostratigraphic value but documents fresh/brackish and warm waters (Esu, 1980), which in our interpretation mark an early Pliocene transitional environment occurring between the SB1 alluvial fan drowning and the marine ingression of the SB2 member.

3.1.2 Structural geology

The bedding attitude of the San Bartolomeo Hill Formation is sub-horizontal and according to the previous studies the whole succession appears to be displaced by a set of NW-trending extensional faults characterized by small vertical offset (Venzo, 1957; Baroni et al., 1995; Picotti et al., 1997). On the basis of the structural analysis of mesoscopic deformation of pebbles, three distinct deformation event were recognized in the San Bartolomeo Hill Formation: an older contractional deformation event with a maximum stress axis ($\sigma 1$) oriented at N45° is followed by two younger extensional deformation phases, with minimum stress axis ($\sigma 3$) oriented at N50° and at N305°, respectively (Picotti et al., 1997). The older extensional event with minimum stress axis ($\sigma 3$) oriented at N45° has interpreted as due to a forebulge tensional stress during the Early Pliocene northward migration of Apennines (Picotti et al., 1997).

Our survey did not provide new data about the normal faults reported in the previous studies. Therefore, the actual contribute of the San Bartolomeo Hill to our tectonic scenario relies on age, elevation, and bedding attitude of the Pliocene deposits coupled with the structural analysis carried out by Picotti et al. (1997).

3.2 Eastern sector

3.2.1 Stratigraphy

Pliocene or early Pleistocene successions were never clearly identified in the eastern Lake Garda bank, with the exception of the Montecio Conglomerate, of generic Neogene age (Venzo, 1961). The conglomerate is exposed at Montecio, close to Sant'Ambrogio di Valpolicella, and along the Cà Verde depression (Fig. 5). It rests with an erosional lower boundary on the bedrock and develops with horizontal and planar cross-bedded, well-sorted, well-rounded, fine-grained gravels. Upsection, the clast size increases up to 25-30 cm and the conglomerate is crudely bedded. The succession ends with a set of gravel-to-sand fining-upward cycles. The overall thickness is ~50 m. Pebbles are composed of limestones and dolostones with few clasts of volcanic and metamorphic rocks. Sand petrography shows abundance of quartz (30 to 45%), limestone (up to 34%) and phyllites (15 to 19%), with a common occurrence of acidic volcanic rocks (up to 11%) (Tab. 3). Facies association suggests that the Montecio Conglomerate was deposited by a shallow, gravel-bed river. The good organization of the body rules out a deposition by a local stream, but rather points to deposition in a braidplain with local high-energy episodes. According to the petrographic composition, the provenance of the Montecio Conglomerate can be constrained to a paleo-river draining the Mesozoic and Tertiary sedimentary cover and volcanic rocks of the east Lake Garda bank, Lessini Mts., and a small portion of the Valsugana basement (Figs. 1 and 4).

Dating the Montecio Conglomerate at Sant'Ambrogio is a hard task due to the lack of fossils and fine-grained layers suitable for pollen or paleomagnetic analyses. Northward, at Rivoli V.se (Fig. 5A), we observed gravels with petrographic composition similar to the Montecio

Conglomerate. The gravel deposit fills tectonic fractures in the Mesozoic bedrock, is strongly weathered, and bears a wealth of fossil microfauna, among which the Late Villanyan *Mimomys pliocaenicus* (Sala et al., 1994), ascribable to the Gelasian (2.59–1.81 Ma; Nomade et al., 2014; Bellucci et al., in press). The petrographic correlation between the Sant'Ambrogio and Rivoli exposures points to a same paleo-drainage (now completely dismembered) for both the deposits and can support their contemporaneity. The Gelasian microfauna at Rivoli is not coeval to the gravels, because the strong weathering would have destroyed the very thin bones. The occurrence of *M. pliocaenicus* should be instead considered penecontemporaneous to the opening of the fractures. Being these bones small, fragile and relatively lightweight, they are usually found in primary deposition as product of nocturnal birds predation activity (e.g., owls), which habitat shelters in rocky and cliffs areas (e.g., Andrews, 1990) compatible with the environment of Rivoli. The *M. pliocaenicus* at Rivoli allows referring the Montecio Conglomerate to a pre-Gelasian time, most likely the Pliocene (see discussion in section 4).

3.2.2 Structural geology

The Montecio Conglomerate fills the NW-oriented Ca' Verde depression and is cut by NW- to WNW-directed fault systems (Fig. 5B). The WNW fault system, which consists of high angle right-lateral faults dipping mainly to NE, is pervasive at meso- to macroscale (Fig. 6B) and is bounded by the NW-directed one. At the mesoscale the faults show a right-stepping *én-echelon* arrangement with meters- to tens-of-meters-wide overlapping zones. Close to the faults, pebble surfaces are polished and locally contain rounded-to elongated solution pits and striae formed by the impact of differently sized pebbles (Fig. 6A). In general, the solution pits occur on opposite poles of the pebbles surface according to the orientation of the maximum compressional stress parallel to their long axis (Caputo et al., 2010, and references therein). Striae and grooves on pebble surfaces vary from parallel to curve on flat surfaces. Grooves are commonly millimeters- to centimeter-long and 0.1-0.2 mm wide, striae are up to 4-5 cm long (Fig. 6A). The direction of both striae and grooves on pitted pebbles is well consistent with that of slickenlines measured on NW faults. Paleostress analysis attempted with the few available data indicates a NNW-SSE orientation (~N175°) of the maximum compressive axis of stress ($\sigma 1$) (Fig. 5C).

Meter-scale, right-lateral faults with an E-W direction also locally occur. The most notable example is a high angle, N-dipping fault consisting of two main surfaces that bound a 50 cm-thick fault breccia (Fig. 6C). Extensional slickenlines occur on the fault surface, representing the reactivation of prevalent right-lateral movements, as indicated by S-C shears within the fault breccia.

In addition to the Sant'Ambrogio area, gravels ascribable to the Montecio Conglomerate fill NE open fractures in the Rivoli V.se area, (Figs. 5, 6D), which cut subvertical NNE-directed, left-lateral faults (Fig. 5C). These open fractures are interpreted, in analogy with what observed at Sant'Ambrogio, as tensile joints produced by right step-overs of the NW-directed right-lateral fault system.

3.3 Central sector

3.3.1 Stratigraphy

The central sector is largely occupied by Lake Garda and by Middle to Late Pleistocene glacial deposits (Cremaschi, 1987). Thankfully, located in the middle of Lake Garda is the Sirmione peninsula (Fig. 7), bearing Late Cretaceous calcareous bedrock (Cita, 1949) and a conglomerate of

uncertain age (Sirmione Conglomerate; Venzo, 1965). The Sirmione Conglomerate is widely exposed along the eastern bank of the Villa Cortine hillock, where it unconformably lies on late Campanian cherty and marly limestones (nannofossil zone CC22c of Sissingh, 1977; Tab. 2). The Sirmione Conglomerate has been attributed to the late Miocene (Venzo, 1965) as well as to the Middle Pleistocene (Cremaschi, 1987) and it is distinguished in two members by facies and sediment composition (Fig. 8). The lower member SIR1 is 11-13 m thick (lower boundary not observed) and consists of massive, coarse-grained, matrix-supported gravel, with boulders from angular (limestones) to rounded (porphyries) shape, passing upward to a crudely-bedded conglomerate, sealed by a massive fine-grained layer, with sandstone lenses and lateral continuity of several tens of meters. The transition to the upper member SIR 2 is gradual and characterized by a 5-6 m-thick interval of crudely bedded, clast-supported conglomerate, showing a better sorting, rounded clasts, and a remarkable minor amount of porphyries. Facies association points to proximal braidplain environment characterized by longitudinal bars and thick debris flow deposits with boulders and blocks up to 1 m size, passing upward to a shallow, gravel-bed river braidplain (Miall, 2006). The SIR 2 member is composed by horizontal to planar, cross-bedded conglomerate, showing well sorting and clast support; pebbles are dominated by limestone and chert. Laminated to massive sandstone lenses occur, more frequently towards the top. Very rare fine-grained layers are thin and observed at the top of sandstone lenses. The dominant horizontal and planar cross-bedded gravel facies association is interpreted as a vertical stack of shallow, gravel-bed river channels, pointing to a braidplain depositional system. The average thickness is 12-15 m, but in the northernmost outcrops the SIR2 member lies directly on the bedrock. Samples collected for pollen analysis in the fine-grained levels were barren.

Sand petrography of the two members shows a clear different provenance (Tab. 1; Fig. 4). SIR1 is polygenic, with a dominance of dolostone fragments (>45%), common limestone (~15%), acidic volcanic (~10%), and metamorphic fragments (~9%). The gradual transition to the upper member shows an increase of limestone grains. Limestones become dominant in SIR2 member (>48%), coupled with cherts (>10%); dolostones are still abundant (~30%), while the other parameters are poorly represented. The comparison with the source areas and available databases (Gazzi et al., 1973; Garzanti et al., 2006; Monegato et al., 2010; Garzanti et al., 2011) points to a Adige catchment provenance for SIR1, as also assessed by the occurrence of granodiorites and gneiss characteristic of the Bressanone area (northeastern sector of the Adige catchment). The SIR2 provenance is conversely related to a smaller drainage, likely located eastwards of the present Lake Garda in the Mesozoic sedimentary cover of the Southern Alps.

Paleoenvironmental and chronologic constraints were obtained by means of pollen and paleomagnetic analyses on the fine-grained layer from the SIR1 member (Fig. 8). Three pollen spectra display the lack of floral elements (e.g., *Tsuga, Carya, Pterocarya*; Tab. 3) widely distributed at the Southern Alps margin during the pre-glacial early Pleistocene (Ravazzi and Rossignol Strick, 1995; Muttoni et al., 2007). Taxa occurring in these samples derived indeed from open conifer forests and steppic scrublands peculiar of the cold and dry climatic conditions that typifies Pleistocene major glacial stages (Muttoni et al., 2003). Samples also yielded abundance of reworked palynomorphs of Pliocene and older time intervals, suggesting a strong erosional input from older terrains. Paleomagnetic analyses on 12 samples show the existence of a low to medium unblocking temperature component, partially or, more frequently, totally superimposed on a high unblocking temperature. The lower unblocking temperature component, removed between room temperature and less than ~600 °C, bears northerly down-pointing inclinations and it is regarded as due to a recent magnetization overprint. The characteristic component, when resolved, is removed to the origin of the demagnetization axes in the temperature range between ~500 °C and ~680 °C and bears a reverse magnetization regarded to be acquired at sediment deposition (DRM). The pervasive normal polarity overprint cannot be interpreted as thermoviscous because the organic matter (i.e. pollen) should have been erased by heat. Therefore, new formation of magnetic mineral

(sulphides and magnetite) during the normal polarity Brunhes chron (<0.78 Ma) is the most likely cause for the normal polarity overprint, thus interpreted as chemical remanent magnetization (CRM). The site mean value, calculated by integrating the analysis of remagnetization circles and the few retrieved paleomagnetic directions (McFadden and McElhinny, 1988), provided dec. = 215° and inc. = -68°.

On the whole, taking into account the pollen results and the paleomagnetic data, the SIR1 member of the Sirmione Conglomerate can be ascribed to a glacial stage of the reverse polarity late Matuyama chron (0.99–0.78 Ma; Muttoni et al., 2003; 2007; Scardia et al., 2010).

3.3.2 Structural geology

Two main fault systems, NW and NE-directed respectively, occur in the Sirmione peninsula. A NE fault displaces the Sirmione Conglomerate along the eastern bank of the peninsula (Fig. 7). It is composed of two main high-angle fault zones, decimeter-to-meter wide and tens-to-hundreds of meter long, each of which consists of several meters long anastomosed faults (Figs. 9A and 9B), with overlapping to overstepping relationships in outcrop. Striated calcite fibers drape the fault surfaces indicating left-lateral movement. Secondary extensional components also occur. Within the overlapping fault segments, pebbles are locally re-oriented and aligned parallel to the faults. Dragging pebbles also occurs in the fault's hanging wall. The same fault system also displaces the Late Cretaceous bedrock. Not-mappable left-lateral faults can be observed in the northern part of the Sirmione peninsula (the "*Grotte di Catullo*" area; Fig. 7), where they show of up to tens-of-meters-long surfaces with positive flower structures in outcrop. Locally, the superposition of striated calcite fibers indicates extensional reactivation of the left-lateral movements.

The second fault system, NW-directed, has been observed only in the Late Cretaceous succession (Fig. 7) and it mainly consists of NE-dipping, right-lateral faults with secondary reverse component of movement. In the northern termination of the Sirmione peninsula, this fault system consists of two main *én echelon* right-stepping faults, hundreds-of-meters long, which are connected by tens-of-meter long N faults (Fig. 7). The main NW fault segment shows horsetail termination at its western tip, displacing with right-lateral movement the NE left-lateral fault observed in the bedrock of the "*Grotte di Catullo*" area (Figs. 9C and 9D). The architecture of the NW fault system strongly resembles that described for the eastern sector in the Sant'Ambrogio area (see section 3.2.2). On the whole, all the observed faults and fractures are consistent with $\sigma 1$ oriented according to a NNW-SSE direction (~N172°) (Fig. 7).

4. Discussion

By integrating stratigraphic and structural data from land exposures with evidence from subsurface geology we interpret a succession of tectonic events recorded along the Southern Alps margin in the Lake Garda area since the Pliocene (Fig. 10).

In the western sector, we recognize and constrain the following deformation phases:

1. **Late Zanclean subsidence and marine transgression**. In our interpretation, this event is materialized by the SB1 deposition and the SB2 marine transgression. It can be considered coeval to a regional stratigraphic event recognized all along the Southern Alps margin and biostratigraphically constrained to the Early Pliocene (Raffi and Rio, 1978; Favero and Grandesso, 1982; Brambilla and Lualdi, 1986, and references therein). At this time the sea penetrated deeply into the Alpine valleys producing a *costa a rias* morphology (Corselli et al., 1985). This regional event can be referred to the intra-Zanclean tectonic phase of Ghielmi et al. (2010), when the northward migration of the Apennine fronts flexed the Alpine orogen, triggering subsidence along the Southern Alps margin and marine transgression into the Alpine valleys. Our biostratigraphic data allow firmly constraining this tectonic event to the late Zanclean at around the NN14–NN15 nannofossil biozones (4.04–3.81 Ma).
2. **Uplift of the San Bartolomeo Hill**. The San Bartolomeo Hill Formation ends with a regressive sequence where braidplain deposits progrades into a coastal/lagoon environment, likely in the latest Zanclean. Somewhere in time since that moment on, i.e. since Piacenzian, the deposits were uplifted to an elevation of ~500 m, providing uplift rate of 0.13 mm/yr. This long-term value is a minimum value as uplift likely started after the deposition of SB3 and it may average a more complex history consisting of more than one phase of uplift and periods of tectonic quiet over a time interval of ~4 m.y. . The uplift is initially produced by a N45° horizontal $\sigma 1$, which can testify an Apennine-driven compressive stress field (Picotti et al., 1997). The two youngest deformations bear vertical $\sigma 1$ and a horizontal $\sigma 3$, which rotates from N50° to N305°. The first N50° extensional deformation event is broadly coaxial to the previous N45° contractional deformation event and documents an inversion of the stress. We interpret this inversion, as well as the development of the normal faults occurring at San Bartolomeo (Fig. 3), as the onset of a tensional stress produced by a bending moment. These structural features can be tentatively explained by the out-of-sequence reactivation of a deep basement structure, which would have deformed the area of the San Bartolomeo Hill in a broad antiform. Within this structure, the San Bartolomeo Hill Formation should lie in the summit because of its sub-horizontal bedding attitude. The following N305° extensional event testifies a further rotation of the stress field, which however continues to trigger the growth of the San Bartolomeo Hill structure. The N305°-directed bending moment is driven by a NW-directed horizontal $\sigma 1$ in good agreement with the maximum stress calculated at Sant'Ambrogio and Sirmione at least since the Gelasian (see below).

In the eastern sector, the following events are reconstructed:

1. **Pre-Gelasian subsidence and deposition of the Montecio Conglomerate.** The occurrence of Gelasian microfauna in association within the Montecio Conglomerate weathered gravels, provides a *terminus ante quem* for the deposition of the Montecio Conglomerate. The thickness of the deposit at Sant'Ambrogio (~50 m) suggests subsidence settings at the Southern Alps margin, consistent with those occurred during the intra-Zanclean phase (Ghielmi et al., 2010) and observed also few tens of kilometers westward at the San Bartolomeo Hill.
2. **Gelasian faulting of the Montecio Conglomerate.** Weathered Montecio Conglomerate is found filling tectonic fractures at Rivoli in association with Gelasian microfauna. This evidence can support a tectonic activity during Gelasian, which created tensile joints, such as those observed in the Montecio Conglomerate at Sant'Ambrogio, and could have likely produced local "pull-

apart" basins bounded by the WNW- to NW-striking right-lateral faults, such as the Cà Verde depression. This deformation is produced by a stress field with NNW horizontal σ1. The Sant'Ambrogio Fault displays some similarity in direction and deformation style with the Nogara Fault detected in seismic lines. Their geometry and kinematics suggest that both belong to the same regional NW-directed "Schio-Vicenza"-like fault system.

In the central sector, the Sirmione Conglomerate recorded the youngest deformation event:

1. **Late Matuyama deposition of the Sirmione Conglomerate.** The conglomerate deposited during one of the earliest glacial stages occurring at the end of the early Pleistocene during the late Matuyama chron, likely in moderate to low subsidence settings.
2. **Middle Pleistocene faulting of the Sirmione Conglomerate.** Due to the latest early Pleistocene age of the Sirmione Conglomerate, we refer the faulting of the Sirmione Conglomerate to the right following Middle Pleistocene. The NE-directed fault observed at Villa Cortine in the Sirmione Conglomerate has roughly the same direction of the underlying Sirmione Fault observed in the subsurface by means of seismic interpretation (Figs. 1 and 2A). Due to the poor exposures at Sirmione, it is still not possible to have a complete picture about the structural relationship between both faults. Taking into account the widely-documented left-lateral transpressive kinematics of the Giudicarie thrust belt (e.g., Picotti et al., 1995; Viganò et al., 2008), we propose as first interpretation that the left-lateral strike-slip fault observed at Villa Cortine can represent the surficial expression of the deeper Sirmione Fault, for which we infer the same left-lateral transpressive kinematics observed in the Giudicarie belt.

On the whole, in our reconstruction of late Alpine tectonics in the Lake Garda area we interpret three distinct deformation events (Fig. 10), recognized and distinguished basing on the different directions of compression and their timing of activity. The oldest corresponds to the intra-Zanclean event of Ghielmi et al. (2010) and it is produced by a severe northward migration of the Apennine fronts. The creation of accommodation space by flexure of the Alpine foreland during this event drives the deposition of the lower conglomerate (SB1) of the San Bartolomeo Hill Formation and, likely, the deposition of the Montecio Conglomerate few tens of kilometers eastward. The marine transgression observed at San Bartolomeo with the SB2 clays marks the maximum flooding surface related to this event at ~4.0 Ma. The intra-Zanclean event can be interpreted according to Caputo et al. (2010) as a period of decoupling along the basal detachment layer of the Apennines critical taper, during which the convergence between Apennines and Alps is accommodated by the frontal propagation of the Apennines thrusts, in agreement with what observed in the subsurface (Ghielmi et al., 2010). The oldest event of contractional deformation observed in the SB1 conglomerate by Picotti et al. (1997) is parallel to the direction of the Northern Apennine migration, suggesting that, after the initial intra-Zanclean propagation of the Apennines thrusts, the stress was transferred through the Adria plate foreland and accommodated by the Alpine margin. This stress transfer is interpreted as produced by coupling along the basal detachment of the Apennines critical taper. In this moment we can constrain the onset of the uplift at the San Bartolomeo Hill and the oldest extensional deformation observed by Picotti et al. (1997). This event can be considered a continuation of the intra-Zanclean deformation phase because σ1 maintains roughly constant, also with regard of the following Gelasian event.

During the Gelasian we observe a radical change of the σ1 direction, which rotates from NE° (N50°) to NNW (~N172°-175°). Similar stress field variations have been documented in the eastern Southern Alps during the last ~10 Ma (Caputo et al., 2003). These variations are interpreted as temporary perturbations of the local stress field in the framework of the remote plate convergence between Africa and Europa and the northeastward migration of Northern Apennines (Caputo et al., 2010). In this geodynamic setting, we interpret the Gelasian stress direction as a result of the vector sum between the stress induced by the NW-oriented Adria plate motion

(Mazzoli and Helman, 1994) and the stress induced by the Apennine northeastward propagation. If during the intra-Zanclean event the latter was the most represented, with the Gelasian event we can assume that both stresses contribute almost equally to produce a NNW-oriented resultant vector for the observed σ1. Probably due to the waning or a change in the deformation style of the Apennine tectonics, the Adria component gets more represented in the σ1 final direction. This new stress regime leads the Gelasian event producing a further tilting in the foreland (Apennine component of deformation), but in addition triggers the onset of strike-slip kinematics in the Lake Garda area with the deformation of the Montecio Conglomerate along the Sant'Ambrogio Fault (Adria component of deformation). The youngest extensional deformation evidence in the San Bartolomeo Hill is roughly coaxial with this new NNW-directed σ1 and is tentatively referred to this event.

Data from the Sirmione Conglomerate show that the NNW-oriented σ1 was also acting during the Middle Pleistocene, when, in agreement with geomorphologic evidence (Desio, 1965; Livio et al., 2009), tectonic deformation is documented in the Lake Garda area. The σ1 we calculated for the Gelasian and Middle Pleistocene events agrees with the direction of maximum compression estimated from the mesostructural analyses in the eastern Southern Alps (Caputo et al., 2010), thus contributing to depict a regional scenario consistent all over a distance of more than 200 km, from the Tagliamento River (at east) to the Lake Garda area (at west).

5. Seismotectonic implications

Our data from subsurface and land exposures led to the recognition of two sets of faults in the Lake Garda area and the Mantova Monocline. One set is characterized by NNE-trending thrust faults, mostly represented in the western sector of the Lake Garda area and ascribable to the Giudicarie belt. The second set is characterized by NW-trending strike-slip faults, observed in the eastern sector and ascribable to a "Schio-Vicenza"-like system. In the Sirmione peninsula, macro- and mesostructures belonging to both sets are observed. The NNE-directed and the NW-directed fault sets bear a left transpressive and a right-lateral strike-slip motion, respectively (Fig. 11). Our kinematic data are in agreement with the focal plane solutions and maximum horizontal stresses provided by Viganò et al. (2008). For instance, the Salò 2004 event (M_w = 5.0) displays a left transpressive motion (Fig. 12). In the seismotectonic perspective, earthquakes in the area of Lessini Mts. should be consistent with a right-lateral strike-slip reactivation of NW-directed faults belonging to the Schio-Vicenza system.

North of Lake Garda, the structural style documented by Castellarin and Cantelli (2000) consists of a NW-directed set of the Schio-Vicenza faults deeply penetrating inside the Giudicarie belt (Fig. 1). The tens-of-km long, NW-directed transfer faults dissect the NNE-trending thrusts and anticlines in short segments, typical of ~10 km or less (Fig. 1). We infer the same structural style in the Lake Garda area, where the NNE-directed Giudicarie thrusts can be likely segmented by the NW-trending "Schio-Vicenza"-like faults detected in the subsurface (i.e. the Nogara Fault) as well as in land exposures (i.e. the Sant'Ambrogio Fault). These NW faults can be interpreted as ancient (Mesozoic?) structures reactivated in the frame of the foreland deformation and kinematically associated to the NNE-directed thrusts of the Lake Garda area (Sirmione and Solferino faults). On the whole, the interplay between the two systems leads to the development of relatively short NNE-directed thrust ramps bounded by longer NW transfer faults with right-lateral strike-slip motion (Fig. 11).

The western sector of Lake Garda experienced earthquakes in the last centuries with comparable level of damage and estimated M_w ranging from 4.6 to 5.5 (Pessina et al., 2013; Fig. 12). The empirical translation of these magnitudes in source length allows estimating thrust ramps with length not exceeding 7 km (Wells and Coppersmith, 1994). The instrumental parameters of the

last event (Salò 2004, M_w = 5.0; Viganò et al., 2008) point to a thrust kinematics with a slight left-lateral component (Fig. 12). Beside the Salò 2004 earthquake, a fragment of the same NNE-trending thrusts may have originated the 1901 earthquake (M_w = 5.5; Pessina et al., 2013; Fig. 12). In this context, even if the macroseismic epicenter of the 1222 earthquake (M_w = 5.8; Locati et al., 2011) is located in Lake Garda (Fig. 12), recent paleoseismologic findings in the Monte Netto Hill (~10 km southeast of Brescia, Fig. 12) indicate the thrust systems in the Brescia area (Malpaga Fault; Fig. 1) as a probable causative source for this event (Livio et al., 2009).

In the seismic history of the Po Plain the most destructive event occurred in 1117 (M_w = 6.7; Fig. 12). Historical information about the damage distribution is sparse and defines significant effects in Cremona, Verona, and Padova (Guidoboni et al., 2007), suggesting a very wide damage area (~150 km between Cremona and Padova; Fig. 1). A possible macroseismic epicenter has been proposed few km south of Verona on the basis of historical data (Locati et al., 2011; Fig. 12). The definition of a seismogenic source is still an open issue, as indicated by the occurrence of different hypotheses. According to Galadini et al. (2005), the 1117 event can be associated to the Thiene-Bassano Thrust, along the front of eastern Southern Alps (Fig. 1). Galli (2005) supported a multi-epicentral hypothesis involving in the 1117 seismic sequence also the buried Piadena Fault along the Apennine front (Fig. 1). Basing on the empirical relationships of Wells and Coppersmith (1994), the estimated magnitude of the 1117 earthquake is produced by a source of ~30-40 km of length. This source length is compatible with the structural style of the Lessini Mts. block and the Mantova Monocline, which are characterized by strike-slip faults traceable for more than 30 km. For instance, the Nogara Fault has been traced on seismic lines for ~60 km and the Sant'Ambrogio Fault length is estimated at least ~30 km (Fig. 1). We then suggest that both faults should be regarded as a potential candidate for the 1117 seismogenic source (Fig. 12).

The Lessini Mts. block also represents the epicentral area of the 1891 earthquake (M_w = 5.8). Although current hypotheses on the origin of this earthquake are not available, the epicentral location in the innermost sector of Lessini Mts. suggests that it originated by the activation of one of the minor strike-slip faults related to the Schio-Vicenza system.

On the whole, by considering the structural framework above discussed and the distribution of the seismicity, the interplay between NNE-directed Giudicarie thrusts and NW-directed "Schio-Vicenza"-like faults is expected to generate moderate magnitude earthquakes (M_w < 6) by the activation of the former and stronger earthquakes (also M_w > 6.5) sourced on the latter.

6. Conclusions

The ongoing convergence between Africa and Europe coupled with the northward migration of the Apennines produced three different tectonic events during the last 5 m.y., namely the intra-Zanclean, Gelasian, and Middle Pleistocene. The former two events, recognized in the subsurface of the Po Plain, left a fingerprint also along the Southern Alps margin in the Pliocene deposits of San Bartolomeo Hill and Sant'Ambrogio di Valpolicella. The youngest event, formerly inferred by geomorphologic and paleoseismologic studies, has been observed and characterized in the Sirmione peninsula.

The intra-Zanclean event produced the southward flexure of the Southern Alps and the marine transgression in the Alpine valleys at ~4.0 Ma. The associated stress was mainly Apennine-driven with a NE direction. Since the Gelasian the maximum compressive axis turned to NNW, keeping this direction also during Middle Pleistocene. The associated deformation has been accommodated by two sets of faults consisting of NNE-trending thrust faults, mostly represented in the western sector of the Lake Garda area and ascribable to the Giudicarie belt, and NW-trending

strike-slip faults, observed in the eastern sector and ascribable to a "Schio-Vicenza"-like system. The interplay between these two sets of faults is interpreted to produce relatively short (< 10 km length) thrust ramps activated in left transpression, bounded by relatively longer (30-60 km) transfer faults activated in a right lateral strike-slip motion.

Basing on our reconstruction we expect moderate seismicity (M_w < 6) associated to the NNE-directed Giudicarie thrusts and stronger earthquakes (also M_w > 6.5) along the NW-trending "Schio-Vicenza"-like strike-slip faults. In this framework, the Nogara Fault or the Sant'Ambrogio Fault could be regarded as potential candidates for the 1117 seismogenic source.

Acknowledgments

This research, developed and funded in the framework of DPC-INGV 2007–2009 agreement (Project S1), benefited from useful discussions by C. Carcano, E. Castellaccio, E.M. Poli, B. Sala, D. Visonà, and R. Zorzin, to whom go our thanks. We also acknowledge ENI E&P for providing subsurface data and Giovanni Muttoni for welcoming GS to use the paleomagnetic facility at the Alpine Laboratory of Paleomagnetism. Finally, we are indebted to R. Cappelletto and M. Colombo for the access and the kind permission of sampling in the Palace Hotel Villa Cortine estate. Paleostress has been calculated with Faultkin (Marrett and Allmendinger, 1990; Allmendinger et al., 2012). The authors are grateful to V. Picotti and the editor Y. Dilek, whose thoughtful revisions greatly improved the manuscript.

References

Allmendinger, R.W., Cardozo, N.C., and Fisher, D., 2012, Structural Geology Algorithms: Vectors & Tensors: Cambridge, Cambridge University Press, 289 p.

Anderson, H., and Jackson, J.A., 1987, Active tectonics of the Adriatic Region: Geophysical Journal of the Royal Astronomical Society, v. 91, p. 937–983.

Andrews, P., 1990, Owls, Caves and Fossils: Chicago, University of Chicago Press, 231 p.

Backman, J., Raffi, I., Rio, D., Fornaciari, E., and Palike, H., 2012, Biozonation and biochronology of Miocene through Pleistocene calcareous nannofossils from low and middle latitudes: Newsletter on Stratigraphy, v. 45, p. 221–244.

Baroni, C., Bissolati, G., and Vercesi, P.L., 1995, Carta Geologica delle Prealpi Bresciane tra la Val Vrenda e il M. Pizzocolo: Atti Ticinesi Scienze della Terra, v. 38, 1 sheet.

Bellucci, L., Bona, F., Corrado, P., Magri, D., Mazzini, I., Parenti, F., Scardia, G., and Sardella, R., in press, Evidence of late Gelasian dispersal of African fauna at Coste San Giacomo (Anagni Basin, central Italy): Quaternary Science Reviews, doi: 10.1016/j.quascirev.2013.10.011

Bertini, A., 2001, Pliocene climatic cycles and altitudinal forest development from 2.7 Ma in the Northern Apennines (Italy): Evidence from the pollen record of the Stirone section (similar to 5.1 to similar to 2.2 Ma): Geobios, v. 34, p. 253–265.

Bertotti, G., Picotti, V., Bernoulli, D., and Castellarin, A., 1993, From rifting to drifting: tectonic evolution of the South-Alpine upper crust from the Triassic to the Early Cretaceous: Sedimentary Geology, v. 86, p. 53–76.

Brambilla, G., and Lualdi, A., 1986, Il Pliocene della Provincia di Bergamo (Italia settentrionale). Analisi faunistica ed inquadramento cronologico e paleoambientale: Bollettino della Società Paleontologica Italiana, v. 25, p. 237–266.

Burrato, P., Vannoli, P., Fracassi, U., and Basili, R., 2012, Is blind faulting truly invisible? Tectonic-controlled drainage evolution in the epicentral area of the May 2012, Emilia-Romagna earthquake sequence (northern Italy): Annals of Geophysics, v. 55, p. 525–531.

Caputo, R., Poli, E., and Zanferrari, A., 2003, Neogene-Quaternary Twist Tectonics in the eastern Southern Alps, Italy: Memorie di Scienze Geologiche 54, 155–158.

Caputo, R., Poli, M.E., and Zanferrari, A., 2010, Neogene-Quaternary Tectonic Stratigraphy of the eastern Southern Alps, NE Italy: Journal of Structural Geology, v. 32, p. 1009–1027.

Carton, A., and Castaldini, D., 1985, Approfondimenti di morfotettonica tra il Lago di Garda ed il Torrente Alpone (Provincia di Verona): Bollettino del Museo Civico di Storia Naturale di Verona, v. 12, p. 461–491.

Cassinis, G., and Perotti, C.R., 1996, Connection between Late Variscan lineaments and Alpine tectonic evolution in Central Southern Alps (Italy). A short review: Notes et Mémoires du Service géologique Maroc, v. 387, p. 125–134.

Castellaccio, E., and Zorzin, R. (eds.), 2012, Acque calde e geotermia della Provincia di Verona: Memorie del Museo Civico di Storia Naturale di Verona, v. 8, 176 p.

Castellarin, A., and Cantelli, L., 2000, Neo-Alpine evolution of the southern Eastern Alps: Journal of Geodynamics, v. 30, p. 251–274.

Castellarin, A., Cantelli, L., Fesce, A.M., Mercier, J.L., Picotti, V., Pini, G.A., Prosser, G., and Selli, L., 1992, Alpine compressional tectonics in the Southern Alps. Relationships with the N-Apennines: Annales Tectonicae, v. 6, p. 62–94.

Cita, M.B., 1949, L'affioramento neocretaceo di Sirmione e la sua microfauna: Rivista Italiana di Paleontologia e Stratigrafia, v. 55, p. 121–134.

Cita, M.B., 1955, Paleogeografia del Terziario nella regione Gardesana: Rivista Italiana di Paleontologia e Stratigrafia, v. 61, p. 137–161.

Corselli, C., Cremaschi, M., and Violanti, D., 1985, Il canyon messiniano di Malnate (Varese), pedogenesi tardo miocenica ed ingressione marina pliocenica al margine meridionale delle Alpi: Rivista Italiana di Paleontologia e Stratigrafia, v. 91, p. 215–236.

Cremaschi, M., 1987, Paleosols and vetusols in the central Po Plain (northern Italy): Milano, Edizioni Unicopli, 306 p.

D'Agostino, N., Avallone, A., Cheloni, D., D'Anastasio, E., Mantenuto, S., and Selvaggi, G., 2008, Active tectonics of the Adriatic region from GPS and earthquake slip vectors: Journal of Geophysical Research B, v. 113, B12413.

Desio, A., 1965, I rilievi isolati della pianura lombarda ed i movimenti tettonici del Quaternario: Rendiconti dell'Istituto Lombardo - Accademia di Scienze e Lettere A, v. 99, p. 881–894.

Esu, D., 1980, Neogene freshwater gastropods and their evolution in the Western Mediterranean area: Geologica Romana, v. 19, p. 231–249.

Fantoni, R., and Franciosi, R., 2010, Tectono-sedimentary setting of the Po Plain and Adriatic foreland: Rendiconti Lincei, v. 21, p. 197–209.

Fantoni, R., Bersezio, R., and Forcella, F., 2004, Alpine structure and deformation chronology at the Southern Alps-Po Plain border in Lombardy: Bollettino della Società Geologica Italiana, v. 123, p. 463–476.

Favero, V., and Grandesso, P., 1982, Nuovi affioramenti di Pliocene marino nei dintorni di Bassano del Grappa (Vicenza): Memorie della Società Geologica Italiana, v. 24, p. 71–77.

Galadini, F., and Galli, P., 1999, Palaeoseismology related to the displaced Roman archaeological remains at Egna (Adige Valley, northern Italy): Tectonophysics, v. 308, p. 171–191.

Galadini, F., Galli, P., Cittadini, A., and Giaccio, B., 2001, Late Quaternary fault movements in the Mt. Baldo-Lessini Mts. sector of the Southalpine area (northern Italy): Geologie en Mijnbouw-Netherlands Journal of Geosciences, v. 80, p. 187–208.

Galadini, F., Poli, M.E., and Zanferrari, A., 2005, Seismogenic sources potentially responsible for earthquakes with M≥ 6 in the eastern Southern Alps (Thiene-Udine sector, NE Italy): Geophysical Journal International, v. 161, p. 739–762.

Galadini, F., Falcucci, E., Galli, P., Giaccio, B., Gori, S., Messina, P., Moro, M., Saroli, M., Scardia, G., and Sposato, A., 2012, Time intervals to assess active and capable faults for engineering practices in Italy: Engineering Geology, v. 139-140, p. 50–65.

Galli, P., 2005, I terremoti del Gennaio 1117. Ipotesi di un epicentro nel cremonese: Il Quaternario, v. 18, p. 87–100.

Garzanti, E., Andò, S., and Vezzoli, G., 2006, The continental crust as a source of sand (Southern Alps cross section, northern Italy): Journal of Geology, v. 114, p. 533–554.

Garzanti, E., Vezzoli, G., and Andò, S., 2011, Paleogeographic and paleodrainage changes during Pleistocene glaciations (Po Plain, Northern Italy): Earth Science Reviews, v. 105, p. 25–48.

Gazzi, P., Zuffa, G.G., Gandolfi, G., and Paganelli, L., 1973, Provenienza e dispersione litoranea delle sabbie delle spiagge adriatiche fra le foci dell'Isonzo e del Foglia: inquadramento regionale: Mem. Soc. Geol. Ital, v. 12, p. 1–37.

Ghielmi, M., Minervini, M., Nini, C., Rogledi, S., Rossi, M., and Vignolo, A., 2010, Sedimentary and tectonic evolution in the eastern Po-Plain and northern Adriatic Sea area from Messinian to Middle Pleistocene (Italy): Rendiconti Lincei, v. 21, p. 131–166.

Gibbard, P.L., Head, M.J., and Walker, M.J.C., 2010, Formal ratification of the Quaternary System/Period and the Pleistocene Series/Epoch with a base at 2.58 Ma: Journal of Quaternary Science, v. 25, p. 96–102.

Guidoboni, E., Ferrari, G., Mariotti, D., Comastri, A., Tarabusi, G., and Valensise, G., 2007. CFTI4Med, Catalogue of Strong Earthquakes in Italy (461 B.C.-1997) and Mediterranean Area (760 B.C.-1500): INGV-SGA.,http://storing.ingv.it/cfti4med/

Laubscher, H., 1985, Large-scale, thin-skinned thrusting in the southern Alps: kinematic models: Geological Society of America Bulletin, v. 96, p. 710–718.

Livio, F., Berlusconi, A., Michetti, A.M., Sileo, G., Zerboni, A., Trombino, L., Cremaschi, M., Mueller, K., Vittori, E., Carcano, C., and Rogledi, S., 2009, Active fault-related folding in the epicentral area of the December 25, 1222 (I_o=IX MCS) Brescia earthquake (Northern Italy): Seismotectonic implications: Tectonophysics, v. 476, p. 320–335.

Locati, M., Camassi, R., and Stucchi, M. (eds.), 2011, DBMI11, the 2011 version of the Italian Macroseismic Database: http://emidius.mi.ingv.it/DBMI11

Lourens, L.J., Hilgen, F.J., Laskar, J., Shackleton, N.J., and Wilson, D.S., 2005, The Neogene Period, in Gradstein, F.M., Ogg, J.G., Smith, A.G., eds., A Geologic Time Scale 2004: Cambridge, Cambridge University Press, p. 409–440.

Marrett, R. A., and Allmendinger, R. W., 1990, Kinematic analysis of fault-slip data: Journal of Structural Geology, v. 12, p. 973–986.

Martini, E., 1971. Standard Tertiary and Quaternary calcareous nannoplankton zonation, in Farinacci, A., ed., Proceedings 2nd International Conference Planktonic Microfossils Roma: Rome (Ed. Tecnosci.) 2, p. 739–785.

Mazzoli, S., and Helman, M., 1994, Neogene patterns of relative plate motion for Africa-Europe: some implications for recent central Mediterranean tectonics: Geologische Rundschau, v. 83, p. 464–468.

McFadden, P.L., and McElhinny, M.W., 1988, The combined analysis of remagnetization circles and direct observations in paleomagnetism: Earth and Planetary Science Letters, v. 87, p. 161–172.

Miall, A.D., 2006, The Geology of Fluvial Deposits: Springer, 582 p.

Monegato, G., Stefani, C., and Zattin, M., 2010, From present rivers to old terrigenous sediments: the evolution of the drainage system in the eastern Southern Alps: Terra Nova, v. 22, p. 218–226.

Muttoni, G., Carcano, C., Garzanti, E., Ghielmi, M., Piccin, A., Pini, R., Rogledi, S., and Sciunnach, D., 2003, Onset of major Pleistocene glaciations in the Alps: Geology, v. 31, p. 989–992.

Muttoni, G., Ravazzi, C., Breda, M., Pini, R., Laj, C., Kissel, C., Mazaud, A., and Garzanti, E., 2007, Magnetostratigraphic dating of an intensification of glacial activity in the southern Italian Alps during Marine Isotope Stage 22: Quaternary Research, v. 67, p. 161–173.

Nomade, S., Pastre, J.-F., Guillou, H., Faure, M., Guérin, C., Delson, E., Debard, E., Voinchet, P., and Messager, E., 2014, $^{40}Ar/^{39}Ar$ constraints on some French landmark Late Pliocene to Early Pleistocene large mammalian paleofaunas: paleoenvironmental and paleoecological implications: Quaternary Geochronology, v. 21, p. 2–15.

Pessina, V., Tertulliani, A., Camassi, R., Rossi, A., and Scardia, G., 2013, The revision of the October 30, 1901 earthquake, west of Lake Garda (northern Italy): Bollettino di Geofisica Teorica ed Applicata, v. 54, p. 77–110.

Picotti, V., Prosser, G., and Castellarin, A., 1995, Structures and kinematics of the Giudicarie - Val Trompia fold and thrust belt (central Southern Alps, northern Italy): Memorie di Scienze Geologiche, v. 47, p. 95–109.

Picotti, V., Bertotti, G., Capozzi, R., and Fesce, A.M., 1997, Evoluzione tettonica quaternaria della Pianura Padana centro-orientale e dei suoi margini: Il Quaternario, v. 10, p. 513–520.

Picotti, V., Capozzi, R., Bertozzi, G., Mosca, F., Sitta, A., and Tornaghi, M., 2007, The Miocene petroleum system of the Northern Apennines in the central Po Plain (Italy), in Lacombe, O., Roure, F., Lavé, J., and Vergés, J. eds., Thrust Belts and Foreland Basins: Springer, 15 pp. 117–131.

Picotti, V., and Pazzaglia, F.J., 2008, A new active tectonic model for the construction of the Northern Apennines mountain front near Bologna (Italy): Journal of Geophysical Research, v. 113, B08412.

Pieri, M., and Groppi, G., 1981, Subsurface geological structure of the Po Plain, Italy: Consiglio Nazionale delle Ricerche, Prog. Fin. Geodin., v. 414, pp. 13.

Raffi, I., and Rio, D., 1978, Il nannoplancton calcareo dell'affioramento pliocenico di Cornuda (Veneto): Acta Naturalia de l'Ateneo Parmense, v. 14, p. 81–94.

Ravaglia, A., Seno, S., Toscani, G., and Fantoni, R., 2006, Mesozoic extension controlling the Southern Alps thrust front geometry under the Po Plain, Italy: Insights from sandbox models: Journal of Structural Geology, v. 28, p. 2084–2096.

Ravazzi, C., and Rossignol Strick, M., 1995, Vegetation change in a climatic cycle of Early Pleistocene age in the Leffe Basin (Northern Italy): Palaeogeography, Palaeoclimatology, Palaeoecology, v. 117, p. 105–122.

Sala, B., Masini, F., and Torre, D., 1994, Villanyian arvicolids from Rivoli Veronese, a karst fissure in the Adige Valley, Northeastern Italy: Bollettino della Società Paleontologica Italiana, v. 33, p. 3–11.

Scardia, G., Muttoni, G., and Sciunnach, D., 2006, Subsurface magnetostratigraphy of Pleistocene sediments from the Po Plain (Italy): Constraints on rates of sedimentation and rock uplift: Geological Society of America Bulletin, v. 118, p. 1299–1312.

Scardia, G., Donegana, M., Muttoni, G., Ravazzi, C., and Vezzoli, G., 2010, Late Matuyama climate forcing on sedimentation at the margin of the southern Alps (Italy): Quaternary Science Reviews, v. 29, p. 832–846.

Scardia, G., De Franco, R., Muttoni, G., Rogledi, S., Caielli, G., Carcano, C., Sciunnach, D., and Piccin, A., 2012, Stratigraphic evidence of a Middle Pleistocene climate-driven flexural uplift in the Alps: Tectonics, v. 31, TC6004.

Sissingh, W., 1977, Biostratigraphy of Cretaceous calcareous nannoplankton: Geologie en Mijnbouw, v. 56, p. 37–65.

Venzo, S., 1957, Rilevamento geologico dell'anfiteatro morenico del Garda - Parte I: Memorie della Società Italiana di Scienze Naturali e del Museo Civico di Storia Naturale di Milano, v. 12, 140 p.

Venzo, S., 1961, Rilevamento geologico dell'anfiteatro morenico del Garda - Parte II: Memorie della Società Italiana di Scienze Naturali e del Museo Civico di Storia Naturale di Milano, v. 13, 64 p.

Venzo, S., 1965, Rilevamento geologico dell'anfiteatro morenico frontale del Garda dal Chiese all'Adige: Memorie della Società Italiana di Scienze Naturali e del Museo Civico di Storia Naturale di Milano, v. 14, 82 p.

Viganò, A., Bressan, G., Ranalli, G., and Martin, S., 2008, Focal mechanism inversion in the Giudicarie-Lessini seismotectonic region (Southern Alps, Italy): Insights on tectonic stress and strain: Tectonophysics, v. 460, p. 106–115.

Wells, D.L., and Coppersmith, K.J., 1994, New empirical relationships among Magnitude, Rupture Length, Rupture Width, Rupture Area, and Surface Displacement: Bulletin of the Seismological Society of America, v. 84, p. 974–1002.

Figures

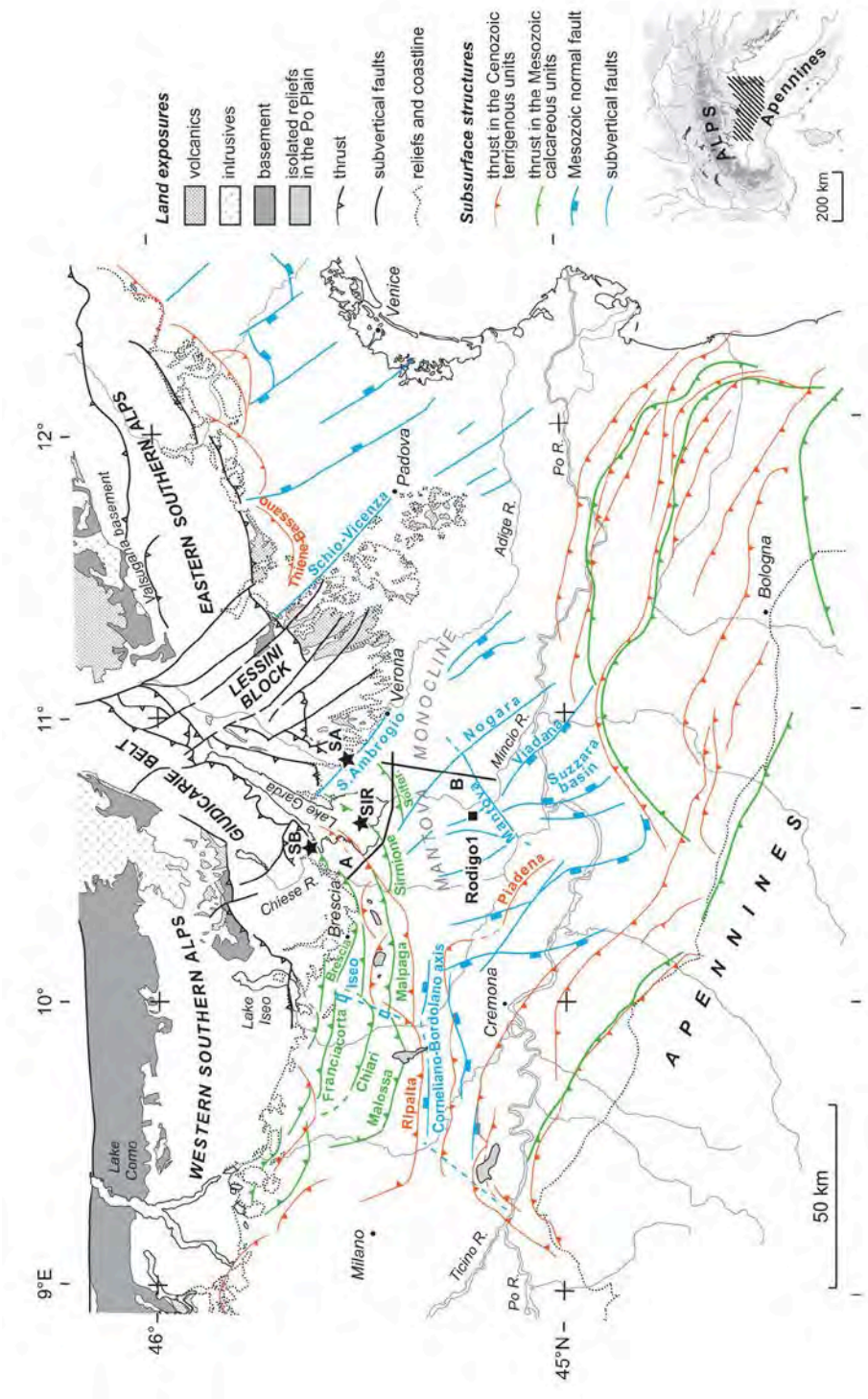

Figure 1 – Structural map of the central-eastern Po Plain with the track of seismic lines A and B, and the Rodigo 1 well (black square) shown in Figure 2. Stars indicate the land exposures where stratigraphic and structural observations were carried out (SB: San Bartolomeo Hill; SIR: Sirmione peninsula; SA: Sant'Ambrogio di Valpolicella).

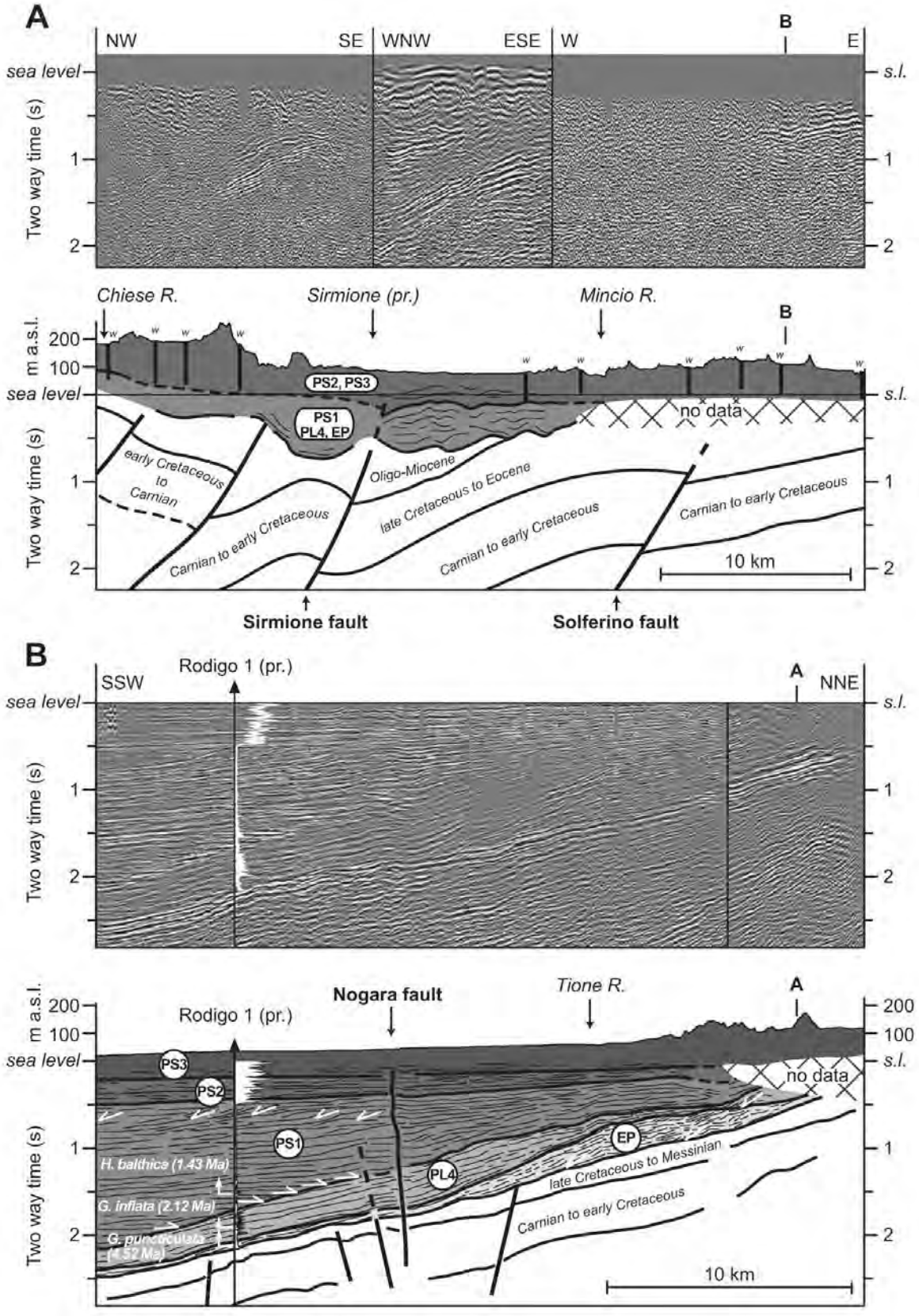

Figure 2 – Representative seismic profiles from the Po Plain and related stratigraphic interpretation. The Rodigo 1 and water wells (*w*) used to calibrate the seismic horizons are also displayed. Ages of biostratigrafic events are from Lourens et al. (2005).

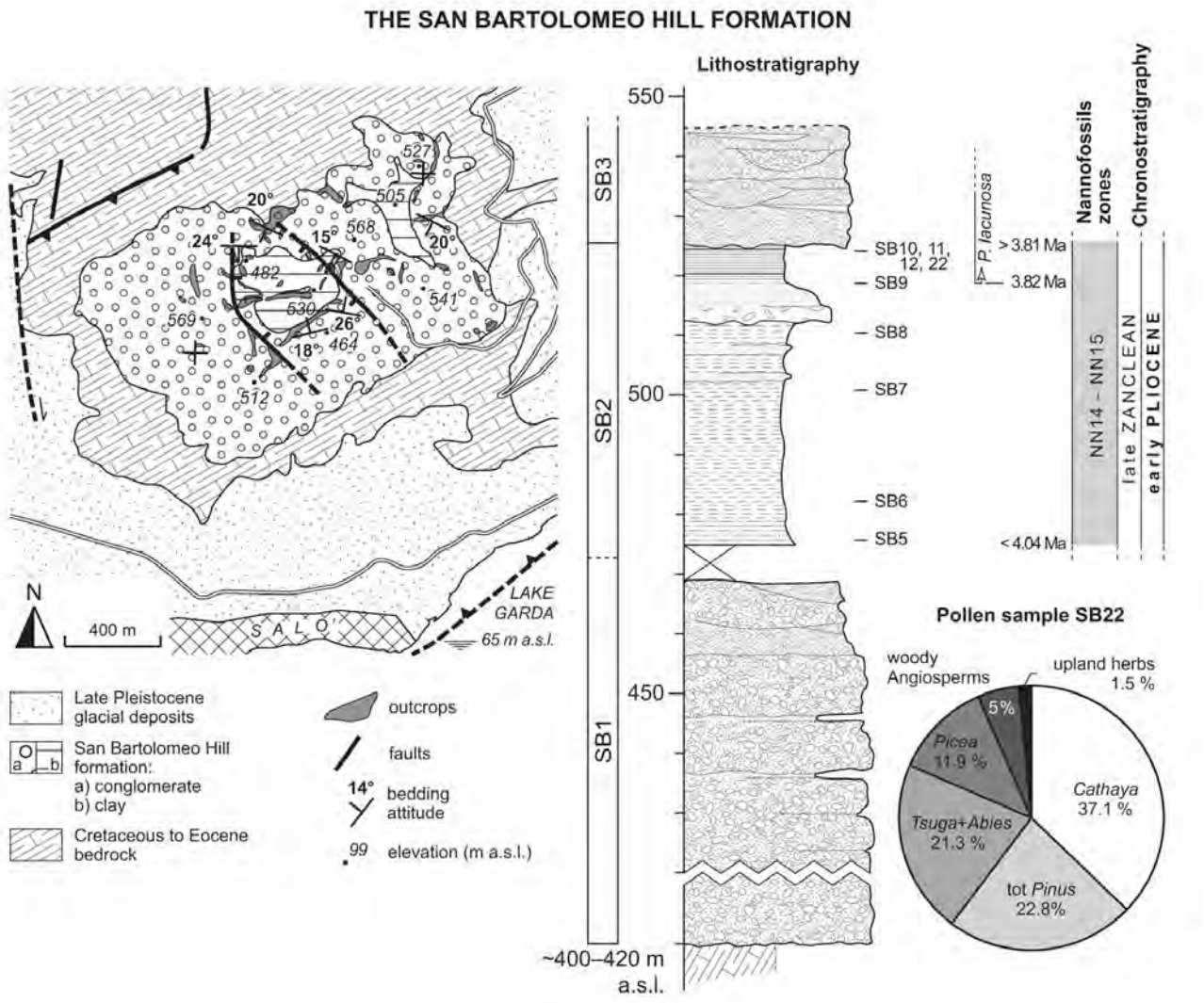

Figure 3 – Geologic sketch, stratigraphy, and biostratigraphic data of the San Bartolomeo Hill Formation. Pollen percentages are based on a sum including pollen in primary deposition of trees, shrubs, and upland herbs.

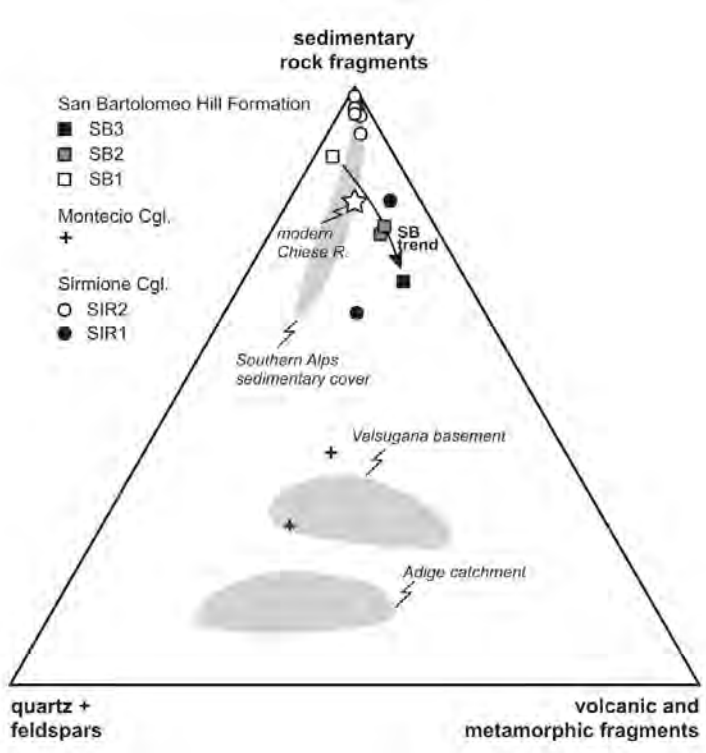

Figure 4 – Ternary diagram showing the petrographic composition of sediments coming from the study sites, compared to Pleistocene fluvioglacial sample and the main source areas represented in 90% confidence field (data from Gazzi et al., 1973; Garzanti et al., 2006; Monegato et al., 2010; Garzanti et al., 2011).

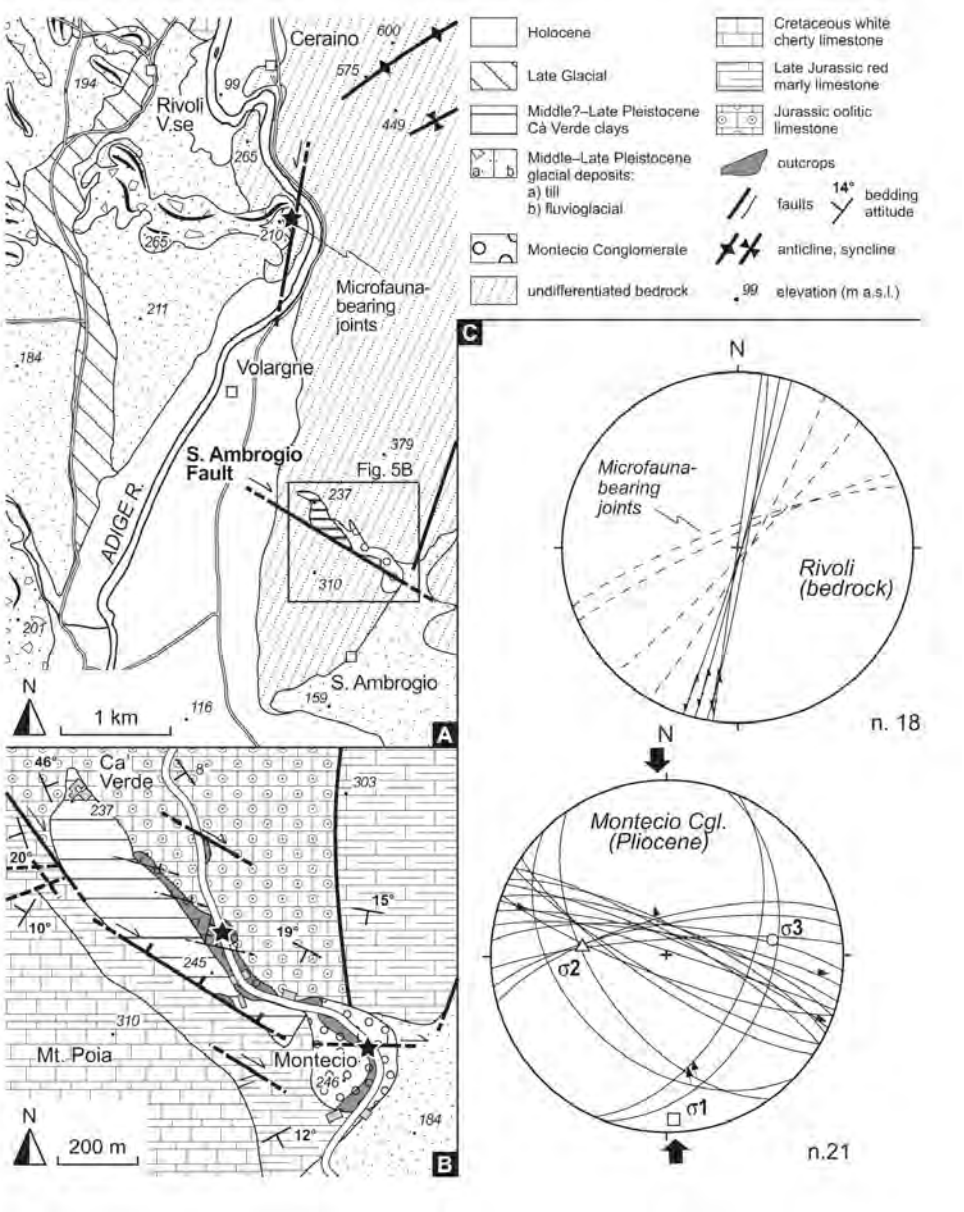

Figure 5 – A: Geologic sketch of the eastern sector of the Lake Garda area. B: Geologic map of the Sant'Ambrogio area. Hatches on the faults indicate the dip of the plane, stars the sites where structural observations were carried out. C: Mesoscale data (Schmidt net, lower hemisphere) of main faults, joints, and deformed pebbles. Black arrows represent the σ1 direction calculated from the structural measurements.

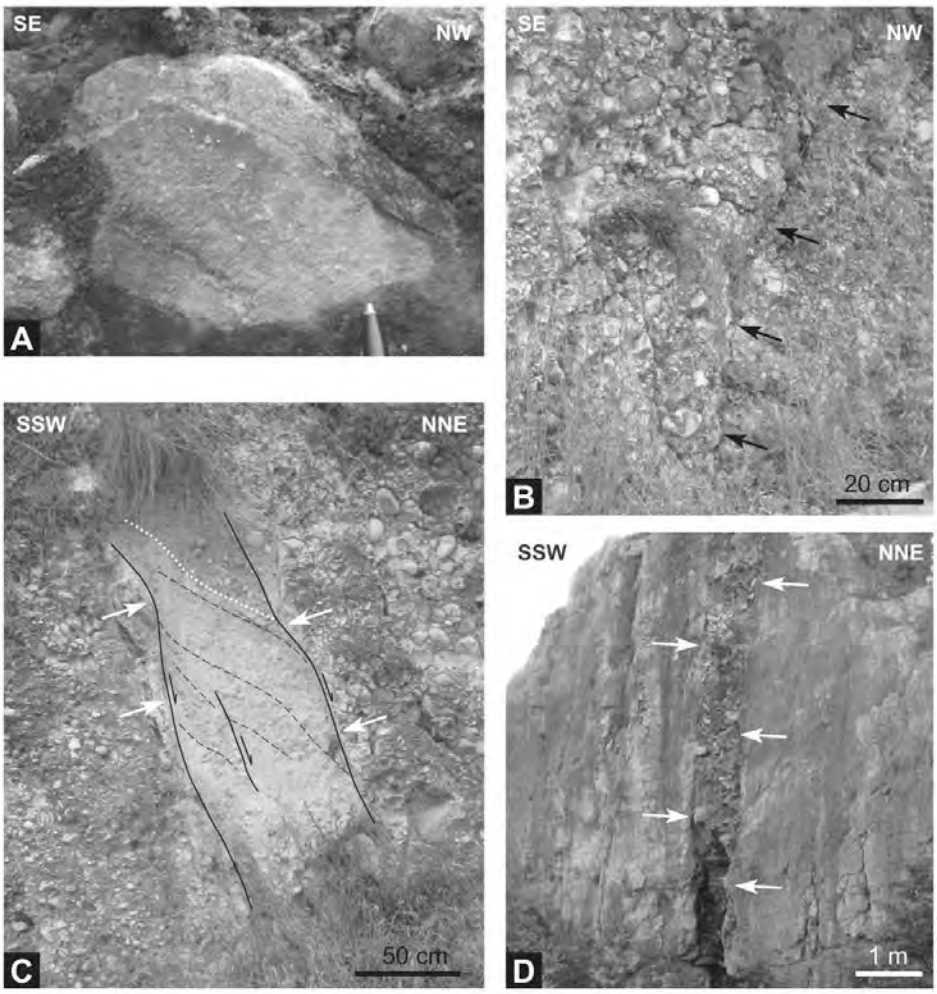

Figure 6 – Evidence of tectonic deformation in the Montecio Conglomerate: (A) Parallel striae on a flat and polished surface of a pebble (pen as scale) related to the WNW fault system, indicated (B) by black arrows (Montecio locality, NE of Sant'Ambrogio). (C) High-angle, N-dipping, normal fault consisting of two main surfaces (white arrows) that bound a 50 cm-thick fault breccia. S-C shears are indicated by black lines (Montecio locality). (D) E-NE striking open fracture filled by the weathered Montecio Conglomerate at Rivoli V.se.

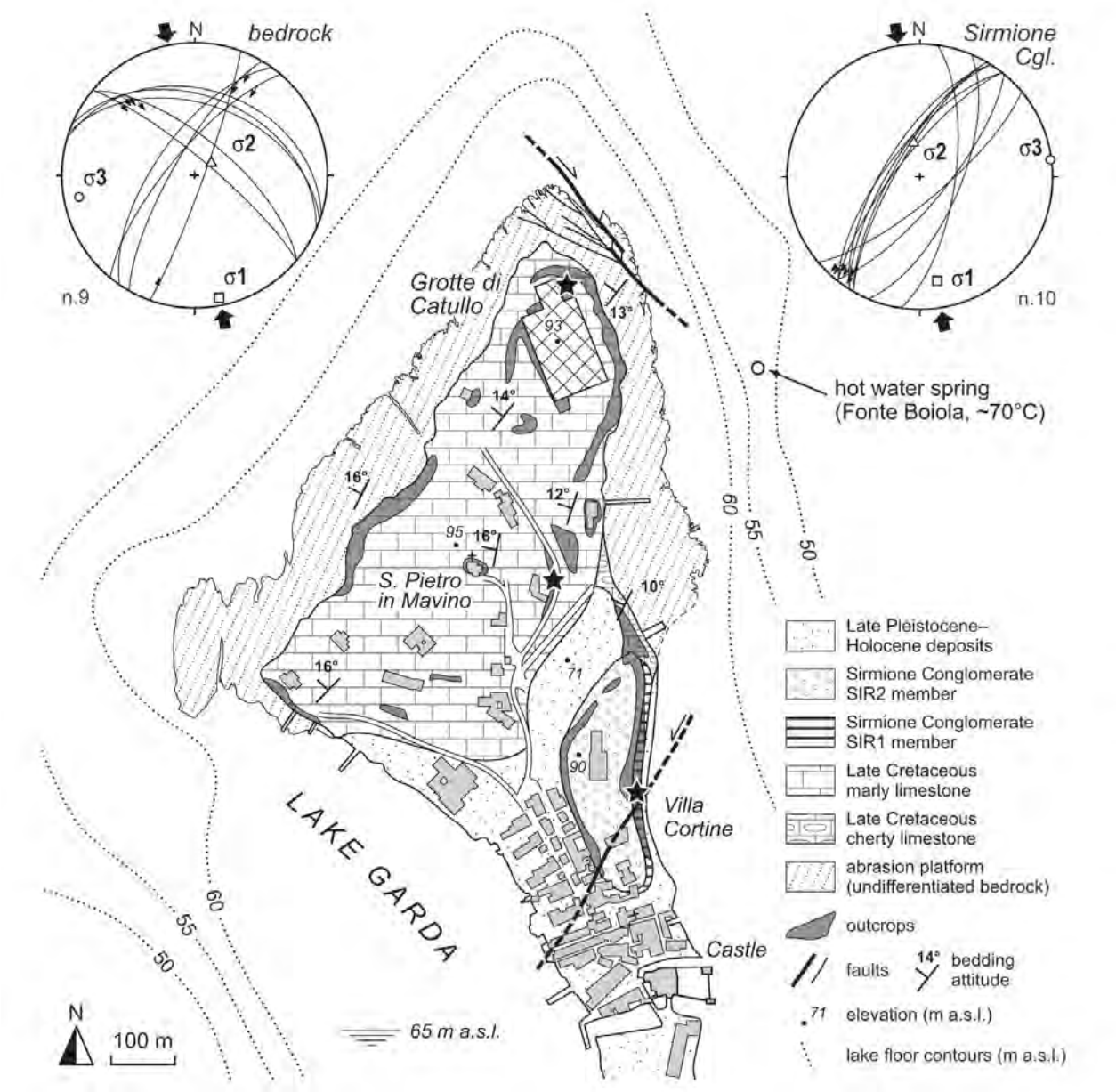

Figure 7 – Geologic map of the Sirmione peninsula. Stars indicate the sites where structural observations were carried out. Insets at the top: mesoscale data (Schmidt net, lower hemisphere) of main faults and deformed pebbles. Black arrows represent the σ1 direction calculated from the structural measurements.

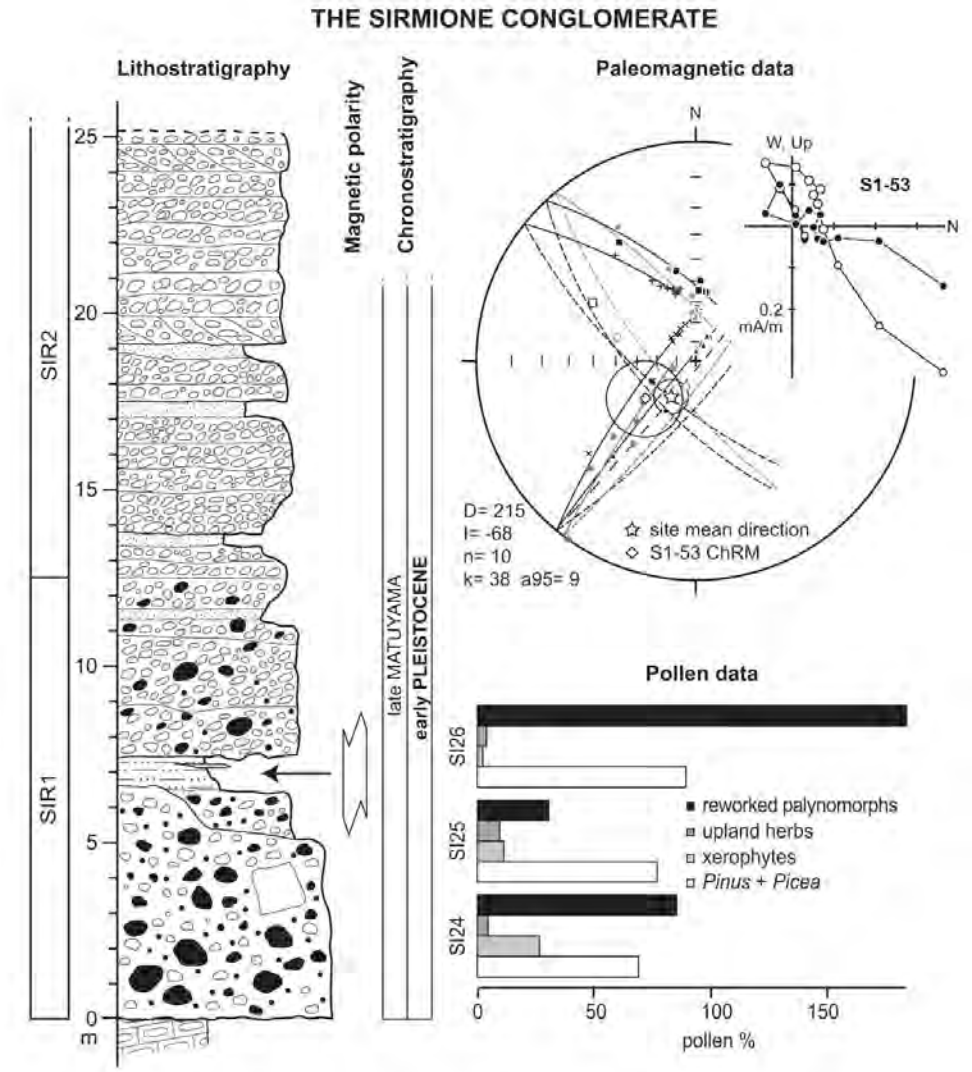

Figure 8 – Stratigraphy, paleomagnetism, and pollen data from the Sirmione Conglomerate. The pelitic level where samples for paleomagnetism and pollen analysis were collected is indicated by arrow. Paleomagnetism: open and closed symbols in the orthogonal vector diagram represent projections onto vertical and horizontal plane, respectively; open and closed symbols in the equal-area projection represent projections onto upper and lower hemisphere, respectively. Star is the site mean value calculated according to McFadden and McElhinny (1988). Pollen percentages are based on a sum including pollen in primary deposition of trees, shrubs, and upland herbs. Xerophytes = sum of *Artemisia*, *Ephedra fragilis* and *E. distachya* types, Hippophae, *Centaurea scabiosa*, *Helianthemum*, Chenopodiaceae; upland herbs = sum of all terrestrial Angiospermes, herbaceous xerophytes excluded.

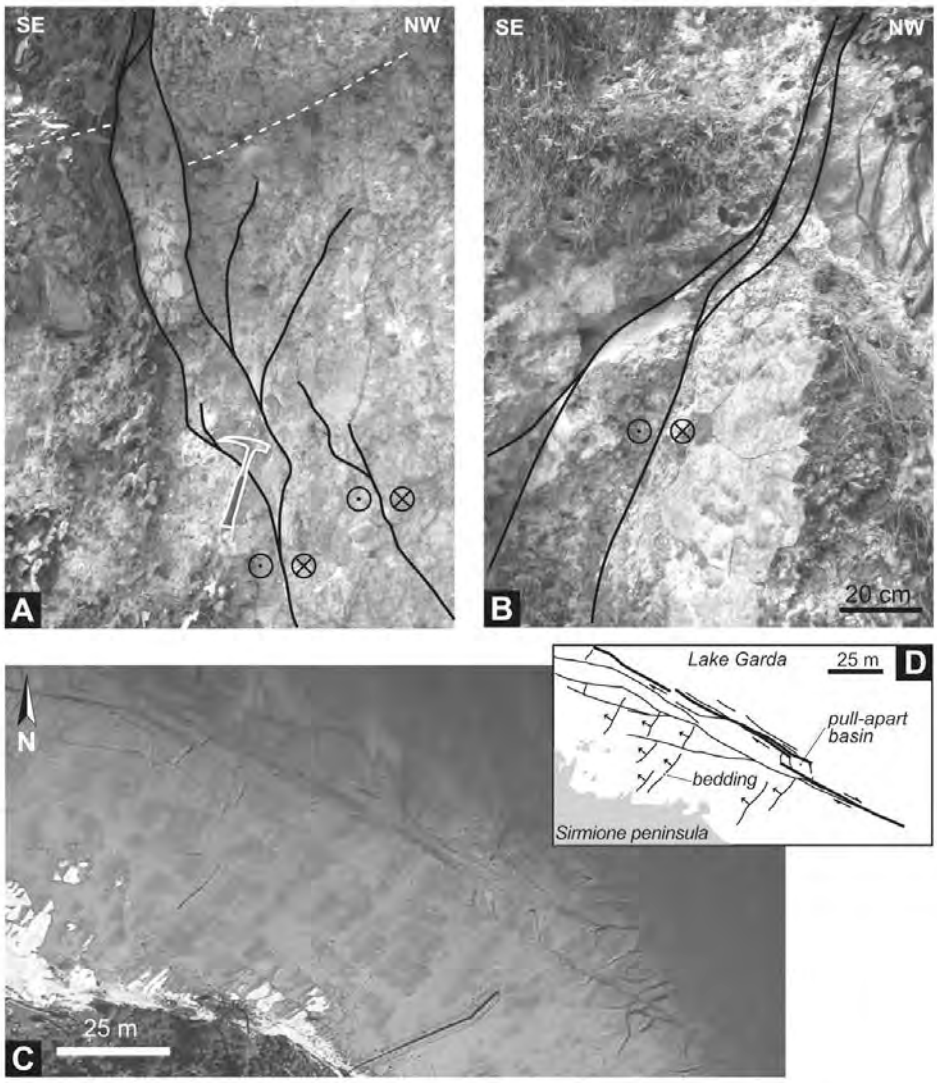

Figure 9 – Evidence of tectonic deformation in the Sirmione peninsula: (A) Left-lateral, NE-striking, high-angle fault zone at Villa Cortine, consisting of several meters long anastomosed faults (black lines) and depicting small-scale flower structures (hammer as scale). Secondary extensional component of movement is shown by the displacement of bedding surfaces (dashed white lines). (B) NE-striking and left-lateral fault, consisting of a decimeters wide shear zone internally characterized by anastomosed fault surfaces (Villa Cortine locality). (C) Aerial photograph of the northern end of the Sirmione peninsula, showing NW-striking, strike slip fault system and the NNE-striking, bedding attitude. Note the northeastern horsetail termination of the NW fault system. (D) Line drawing of panel C.

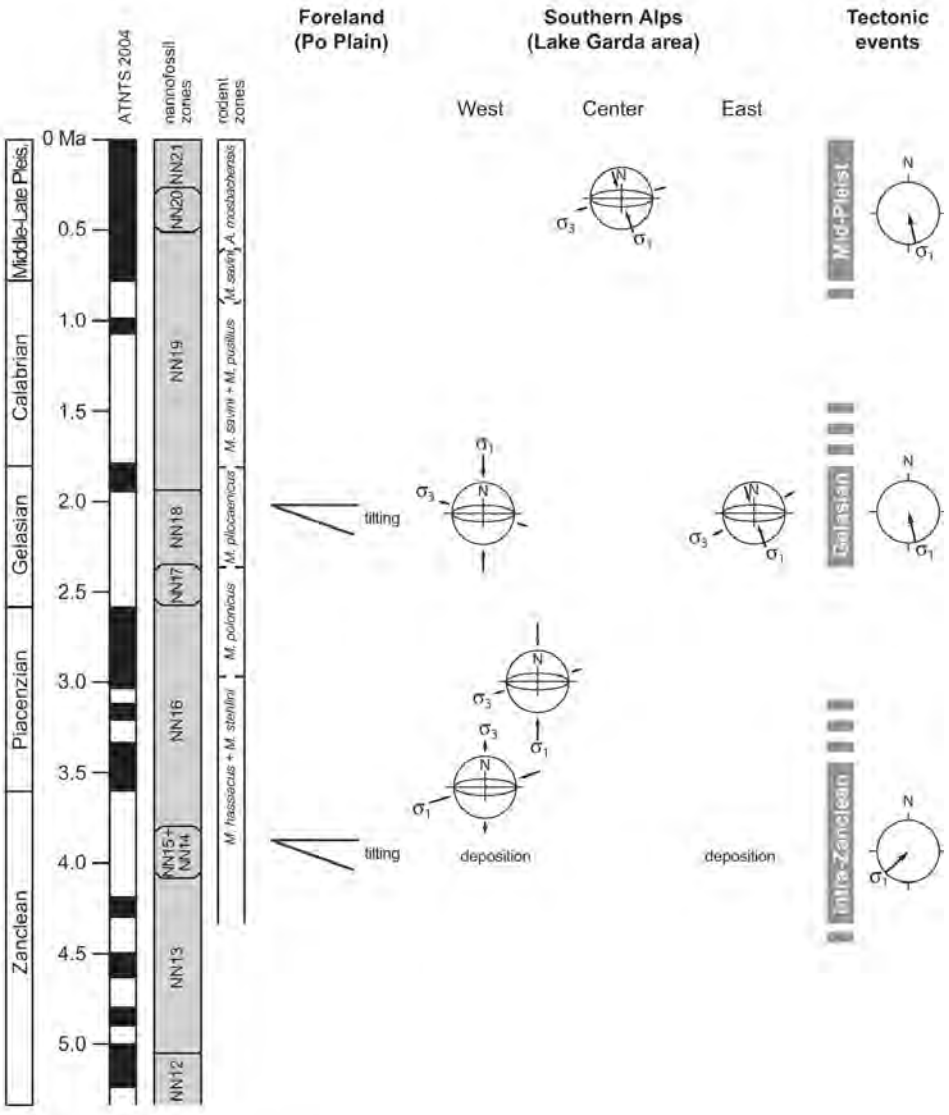

Figure 10 - Synthetic diagram showing deformation and age of the tectonic events recognized in the Po Plain (Ghielmi et al., 2010) and along the Southern Alps margin in the Lake Garda area. The direction of maximum compression estimated from the mesostructural analyses (σ1) is also reported.

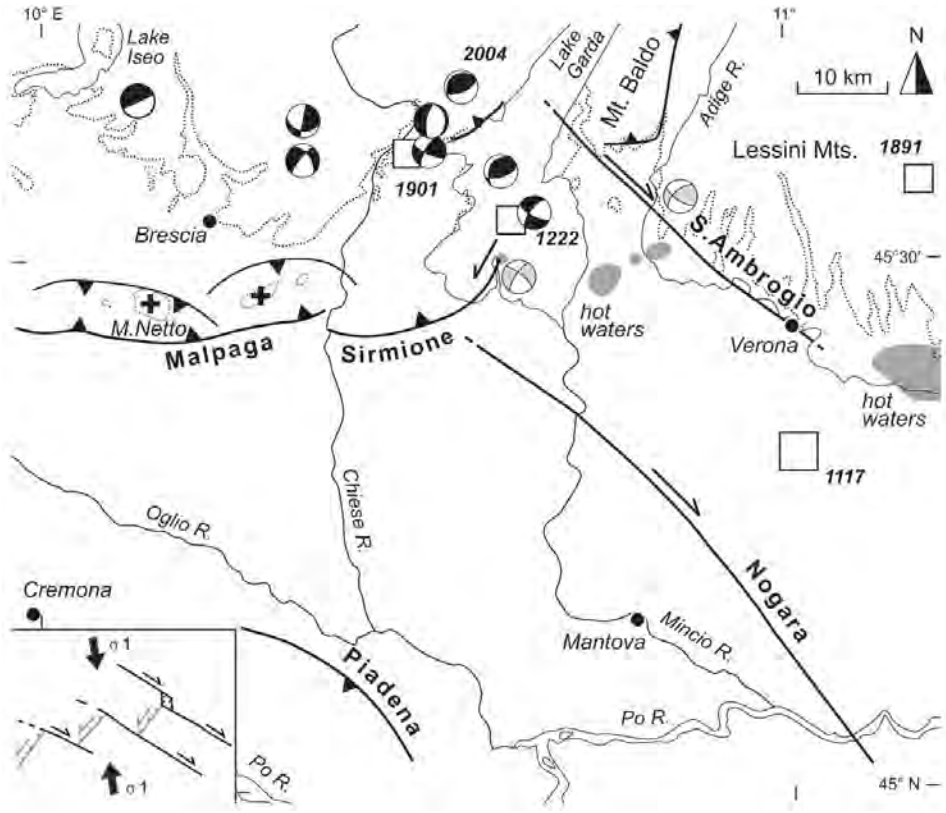

Figure 12 – Seismotectonic model of the central Po Plain. Faults displaying activity during the Pleistocene are reported from Galadini et al. (2001), Galli (2005), Livio et al. (2009), and this study. The focal plane solutions are from Viganò et al. (2008), macroseismic epicenters of historical earthquakes (squares) are from DBMI11 (Locati et al., 2011). The P-T diagrams for Sirmione and Sant'Ambrogio (in grey) have been calculated by the structural and kinematics data presented in Figs. 5 and 7. Crosses indicate the isolated reliefs of the Po Plain produced by active fault-related folding. Shaded area shows the vent of hot waters after Castellaccio and Zorzin (2012).

Tables

TABLE 1. DETRITAL MODES OF PLIOCENE–PLEISTOCENE SANDSTONES FROM THE LAKE GARDA AREA

Unit:	San Bartolomeo Hill Formation				Montecio Conglomerate			Sirmione Conglomerate								
Member:	SB1	SB2		SB3				SIR1			SIR2					
Sample:	SB18	SB20	SB21	SB24	SA1	SA2	SA3	SIR13	SIR11	SIR17	SIR1	SIR2	SIR5	SIR6	SIR7	SIR8
Q	2.2	5.6	5.2	6.0	7.1	45.1	30.8	3.1	4.4	17.7	1.6	1.6	1.3	1.5	0.9	2.2
Kf	0.3	3.1	2.4	2.7	0.9	1.0	2.8			0.6				0.3		
P							0.3			0.3						
Lvf	7.6	10.9	10.5	17.6	5.6	5.9	11.2	4.0	13.2	8.2	1.9	3.2	1.3	1.5	0.3	1.6
Lvi			0.3				0.6			0.3						
Lvb					0.6	0.7	0.3									
Lvp								0.9	0.8	1.8						
Lcc	25.1	19.7	18.4	27.1	77.2	16.8	34.7	62.7	18.7	10.8	51.5	55.5	49.4	48.0	49.6	47.8
Lcd	57.3	49.7	47.9	27.4	0.9	2.4	0.8	14.3	61.0	45.9	23.2	25.6	32.1	30.7	35.9	35.1
Lp	6.0	6.0	10.2	14.6	1.8	6.6	2.2	3.1	1.4	4.0	6.7	2.6	1.6	6.4	3.7	4.8
Lch	0.6				2.1	0.7	1.1	11.8		1.3	14.5	11.4	13.8	11.4	9.4	7.8
Lms	0.9	4.4	2.7	4.6	3.5	19.6	14.8		0.5	7.9	0.6		0.5	0.3	0.3	0.6
Lmi		0.6	2.4		0.3	1.0	0.3			1.1						

Note: Q—quartz; Kf—K-feldspar; P—plagioclase; Lvf—felsic volcanic and subvolcanic lithic fragments; Lvi—intermediate volcanic and subvolcanic lithic fragments; Lvb—basic volcanic and subvolcanic lithic fragments; Lvp—plutonic lithic fragments; Lcc—limestone grains; Lcd—dolostone grains; Lp—shale, siltstone lithic fragments, Lch—chert grains; Lms—low-grade metamorphic lithic fragments; Lmi—medium-grade metamorphic lithic fragments.

Table 1 – Detrital modes of Plio-Pleistocene sandstones from the Lake Garda area. Q: quartz; Kf: K-feldspar; P: plagioclase; Lvf: felsic volcanic and subvolcanic lithic fragments; Lvi: intermediate volcanic and subvolcanic lithic fragments; Lvb: basic volcanic and subvolcanic lithic fragments; Lvp: plutonic lithic fragments; Lcc: limestone grains; Lcd: dolostone grains; Lp: shale, siltstone lithic fragments; Lch: chert grains; Lms: low-grade metamorphic lithic fragments; Lmi: medium-grade metamorphic lithic fragments.

TABLE 2. NANNOFOSSIL DISTRIBUTION CHART FOR THE SAN BARTOLOMEO HILL FORMATION AND THE BEDROCK OF THE SIRMIONE PENINSULA ("SCAGLIA" FACIES)

	San Bartolomeo Hill Formation, SB2 member							
Sample:	SB5	SB6	SB7	SB8	SB9	SB10	SB11	SB12
Preservation:	M	P	M	M	M	M	P	M
Abundance:	F	R	R	R	R	R	R	R
Braarudosphaera bigelowii					1			
Calcidiscus leptoporus	2		1	1	1	1		1
Coccolithus pelagicus	6	1	5	4	7	8	2	4
Helicosphaera carteri	5	1	2	1	6	7	1	9
Helicosphaera sellii	2		1		1	1		1
Pseudoemiliania lacunosa					2	2	1	2
Reticulofenestra minuta group	16	3	11	12	10	18	5	6
Reticulofenestra pseudoumbilica	33	6	19	22	10	13	5	3
Pseudoemiliana ovata	2		1	1	1	1		
Calcidiscus macintyrei	1			1				1
Discoaster spp.	1			1				2
Sphenolithus abies	5	1		2		3	1	2
Umbilicosphaera jafari	1			1				
Discoaster variabilis						1		
Reworked Cretaceous	21	4	19		31	44	5	31
Reworked Paleogene			4		11	12	2	8
Calcareous nannofossil zone (Martini, 1971)	NN14	NN14	NN14	NN14	NN15	NN15	NN15	NN15

	Sirmione peninsula bedrock (Scaglia)				
Sample:	SCA6	SCA4	SCA1	SCA2	SCA3
Preservation:	M	P	P	P	M
Abundance:	F	R	R	R	F
Arkhangelskiella cymbiformis	1	1	1	1	1
Broinsonia parca	1	1	1		1
Chiastozygus litterarius	1	1	1		1
Cretarhabdus conicus	1				1
Cribrosphaerella ehrenbergii	3	1	2	1	1
Cylindralithus spp.	1				
Eiffellithus eximius	1	2	1	1	1
Eiffellithus turriseiffelii	1	1	1	1	1
Gartnerago segmentatum	1		1		1
Microrhabdulus decoratus	1				
Micula staurophora	1	1	1	1	1
Prediscosphaera cretacea	1	1	1	1	1
Prediscosphaera spinosa	1	1		1	
Quadrum gartneri	1	1	1	1	1
Reinhardtites anthophorus	1	1		1	1
Retecapsa crenulata	3	1	1		1
Retecapsa schizobrachiata	1	1			
Staurolithites crux	1				
Tegumentum stradneri	1		1		1
Tranolithus orionatus	1	1	1	1	1
Watznaueria barnesae	5	1	1	3	4
Zeugrhabdotus elegans	1	1			
Zeugrhabdotus embergeri	1	1			1
Zeugrhabdotus erectus	1				
Gartnerago obliquum		1			
Hexalithus gardetiae		1	1		1
Kamptnerius magnificus		1			1
Lucianorhabdus cayeuxii					1
Reinhardtites levis	1		1	1	1
Zeugrhabdotus diplogrammus					1
Quadrum trifidum	1			1	
Calcareous nannofossil zone (Sissingh, 1977)	CC22c	CC22c	CC22c	CC22c	CC22c

Note: Abundance is expressed as F (frequent) and R (rare), preservation as M (moderate) and P (poor).

Table 2 – Nannofossil distribution chart for the San Bartolomeo Hill Formation and the bedrock of the Sirmione peninsula ("scaglia" facies). Abundance is expressed as F (frequent) and R (rare), preservation as M (moderate) and P (poor).

TABLE 3. POLLEN DATA (RAW COUNTS AND PERCENTAGE VALUES) FOR THE SAN BARTOLOMEO HILL FORMATION AND THE SIRMIONE CONGLOMERATE

	Sirmione						San Bartolomeo	
	SI 24		SI 25		SI 26		SB 22	
	grains	pollen %	grains	pollen %	grains	pollen %	grains	pollen %
Gymnosperms								
Pinus sylvestris/mugo	211	52	266	65.8	62	58.5		
Pinus cembra	17	4.2	10	2.5	9	8.5		
Pinus Diploxylon type							41	20.3
Pinus Haploxylon type							5	2.5
Picea	54	13.3	35	8.7	24	22.6	24	11.9
Abies			3	0.7	4	3.8	19	9.4
Cathaya							75	37.1
Tsuga							24	11.9
Sciadopitys							1	+
Ephedra distachya type	76	18.7	9	2.2				
Ephedra fragilis type	7	1.7						
Total Gymnosperms	365	89.9	323	80	99	93.4	189	93.6
Woody Angiosperms								
Alnus glutinosa type			1	+	1	+	3	1.5
Betula			4	1			1	+
Carpinus orientalis							1	+
Ericaceae							1	+
Fagus							2	1
Hippophae	2	0.5	12	3				
Juglans							1	+
Deciduous *Quercus*							1	+
Tilia	1	+						
Total woody angiosperms	3	0.7	17	4.2	1	+	10	5
Upland herbs								
Gramineae	8	2	21	5.2				
Anthemis type			1	+				
Centaurea scabiosa	4	1	3	0.7				
Artemisia	13	3.2	20	5	2	1.9	1	+
Cichorioideae	9	2.2	15	3.7	4	3.8	1	+
Chenopodiaceae	1	0.2	2	0.5				
Helianthemum	5	1.2						
Caryophyllaceae			1	+				
Umbelliferae			1	+				
Polygonum viviparum	1	+						
Cruciferae							1	+
Total upland herbs	41	10.1	64	15.8	6	5.7	3	1.5
Aquatic and wetlands								
Cyperaceae	2	0.5	1	+				
Epilobium	3	0.7	4	1				
Thalictrum								
Total aquatic and wetlands	5	1.2	4	1				
Reworked palynomorphs								
Picea	22	5.4	9	2.2	13	12.3		
Pinus	312	76.8	111	27.5	164	154.7		
Abies	1	+			2	1.9		
cf *Cathaya*	6	1.5	1	+	7	6.6		
Cedrus					1	+		
Classopollis	5	1.2	1	+	2	1.9		
Unidentified 4-porate	1	+						
Unidentified 3-porate			1	+	1	+		
Taxodiaceae					1	+		
Cf. *Corylus*					1	+		
Carbonized *Pinus*					3	2.8		
3-porate cf. *Carya*	1	+						
Total reworked palynomorphs	348	85.7	123	30.4	195	184		
Non pollen palynomorphs (sensu van Geel, 1978)								
Glomus					11	10.4		
Pteridophytes								
Monolete spores							7	3.5
Pteris							3	1.5
Marine microfossils								
Cysts of Dinoflagellata	6	1.5			8	7.5	1	+
Pollen sum (aquatic and wetlands excluded)	406		404		106		202	
Pollen sum (aquatic and wetlands included)	411		408		106		202	
Total number of taxa	17		18		7		17	
Pollen concentration (grains/cm³)	14,315		11,232		555		1794	
Charcoal concentration (part./cm²)	723		413		185		35	
Reworked palynomorph concentration (grains/cm³)	11,975		3386		2371		/	

Note: Pollen percentages are based on a pollen sum consisting of trees, shrubs, and upland herbs. Pollens of aquatic/wetland species, reworked, and nonpollen palynomorphs, Pteridophyte spores, and marine microfossils are excluded from the main pollen sum.

Table 3 – Pollen data (raw counts and percentage values) for the San Bartolomeo Hill Formation and the Sirmione Conglomerate. Pollen percentages are based on a pollen sum consisting of trees, shrubs and upland herbs. Pollen of aquatic/wetland species, reworked and non-pollen palynomorphs, Pteridophytes spores and marine microfossils are excluded from the main pollen sum.